

ROBERT KOCH INSTITUT



Originally published as:

Yao, G., Zhang, S., Mahrhold, S., Lam, K.-H., Stern, D., Bagramyan, K., Perry, K., Kalkum, M., Rummel, A., Dong, M., Jin, R.

N-linked glycosylation of SV2 is required for binding and uptake of botulinum neurotoxin A (2016) Nature Structural and Molecular Biology, 23 (7), pp. 656-662.

DOI: 10.1038/nsmb.3245

This is an author manuscript.

The definitive version is available at: <http://www.nature.com/nsmb/index.html>

1 **N-linked glycosylation of SV2 sweetens the uptake of**
2 **botulinum neurotoxin A1**

3
4 Guorui Yao^{1†}, Sicai Zhang^{2†}, Stefan Mahrhold^{3†}, Kwok-ho Lam¹, Daniel Stern⁴, Karine
5 Bagramyan⁵, Kay Perry⁶, Markus Kalkum⁵, Andreas Rummel^{3*}, Min Dong^{2*}, Rongsheng Jin^{1*}

6
7 ¹ Department of Physiology and Biophysics, University of California, Irvine, CA 92697, USA.

8 ² Department of Urology, Boston Children's Hospital, Department of Microbiology and
9 Immunobiology and Department of Surgery, Harvard Medical School, Boston, MA 02115, USA.

10 ³ Institut für Toxikologie, Medizinische Hochschule Hannover, Carl-Neuberg-Str. 1, 30625
11 Hannover, Germany.

12 ⁴ Centre for Biological Threats and Special Pathogens - Biological Toxins (ZBS3), Robert Koch-
13 Institut, Seestr. 10, 13353 Berlin, Germany.

14 ⁵ Beckman Research Institute of City of Hope, Department of Molecular Immunology, Duarte,
15 CA 91010, USA.

16 ⁶ NE-CAT and Department of Chemistry and Chemical Biology, Cornell University, Building
17 436E, Argonne National Laboratory, 9700 S. Cass Avenue, Argonne, IL 60439, USA.

18
19
20 *Correspondence to: R.J. (r.jin@uci.edu), M.D. (min.dong@childrens.harvard.edu), or A.R.
21 (rummel.andreas@mh-hannover.de).

22 † These authors contributed equally to this work.
23

24 **ABSTRACT**

25 Botulinum neurotoxin serotype A1 (BoNT/A1) is well adapted to invade motoneurons. Here we
26 report a 2.0 Å resolution crystal structure of BoNT/A1 receptor-binding domain in complex with
27 its neuronal receptor, the glycosylated human SV2C. We find that the remarkable neuronal
28 tropism of BoNT/A1 is only achieved by directly recognizing both the peptide moiety and an N-
29 linked glycan on SV2. This N-glycan—conserved in all SV2 isoforms across vertebrates—is
30 essential for BoNT/A1 binding to neurons and its potent neurotoxicity. Remarkably, the glycan-
31 binding interface is largely conserved in a newly identified mosaic toxin BoNT/HA (also known
32 as mosaic BoNT/FA), and it is also the targeting site for a potent human BoNT/A1-neutralizing
33 antibody that is currently licensed as an anti-botulism drug. Collectively, our studies reveal a
34 new paradigm of host-pathogen interactions, in which pathogens exploit conserved host post-
35 translational modifications to achieve highly specific receptor binding while also tolerating
36 genetic changes across multiple isoforms of receptors.

37 BoNT/A1 is one of the most dangerous potential bioterrorism agents. Ironically, it is a licensed
38 drug widely used in treating a variety of medical and cosmetic conditions¹. According to a well-
39 accepted dual-receptor model, the extreme potency of BoNT/A1 targeting motoneurons is
40 mediated by its receptor-binding domain (H_CA), which synergistically binds to host protein
41 receptors and gangliosides on the neuronal surface at neuromuscular junctions²⁻⁴. The synaptic
42 vesicle glycoprotein 2 (SV2), a family of 12-transmembrane domain proteins that have three
43 isoforms (SV2A, 2B, and 2C) in humans, are protein receptors for BoNT/A1^{5,6}, as well as for
44 BoNT/E⁷, BoNT/D⁸, and BoNT/F^{9,10}.

45 We have previously mapped the BoNT/A1-binding site to the fourth luminal domain of SV2s
46 (SV2-L4)^{5,6}. A crystal structure of H_CA in complex with the recombinant human SV2C-L4
47 expressed in *E. coli* (referred to as bSV2C with b indicating bacterial expression) has been
48 reported recently¹¹. It shows that H_CA-bSV2C recognition relies mostly on backbone-to-
49 backbone interactions within a small interface (~596 Å²), mediated by two β-strands in H_CA and
50 one open edge of the quadrilateral β-helices of bSV2C¹¹. This binding mode is in sharp contrast
51 to BoNT/B, which recognizes its receptors synaptotagmin-I/II (Syt-I/II) through an extensive
52 side-chain mediated protein-protein interaction network that ensures high binding affinity and
53 specificity towards Syt-I/II^{12,13}. So, how could BoNT/A1 possibly achieve extreme efficacy of
54 targeting neurons using mostly backbone-mediated interactions for receptor recognition?

55 In this study, we determined the crystal structures of H_CA in complex with rat bSV2C-L4 and the
56 physiologically more relevant glycosylated human SV2C-L4. We found that BoNT/A1
57 recognizes two distinct structural elements on SV2C: the protein moiety and an N-linked glycan
58 that is conserved in all known SV2 homologs across vertebrates. Further biophysical, cellular
59 and functional studies demonstrate that SV2 glycans are essential for BoNT/A1 binding to
60 neuron and its extreme toxicity at its physiological site of action, the motor nerve terminals.
61 Moreover, we found that the glycan-binding site of BoNT/A1 is also the target of a potent human
62 neutralizing antibody, suggesting the potential for SV2 glycan as a novel target for developing
63 BoNT inhibitors.

64

65 RESULTS

66 The crystal structure of H_CA in complex with rat bSV2C

67 Amino acid sequence analyses showed that even the few residues that mediate side-chain
68 interactions in the H_CA and human bSV2C complex are not strictly conserved in SV2A and
69 SV2B, or even SV2C from other species (e.g. rodents) (**Supplementary Fig. 1**). To gain a better
70 insight into how BoNT/A1 can recognize SV2C from different species, we determined the
71 crystal structure of H_CA in complex with rat SV2C-L4 expressed in *E. coli* (**Table 1**). The
72 structure of the rat bSV2C-H_CA complex is virtually identical to that of the human bSV2C
73 complex [root mean square deviation (RMSD) ~ 0.70 Å over 496 aligned C α pairs]. Two major
74 differences are observed. First, H_CA-R1294 forms hydrogen bonds with S519, C520, T521, and
75 D539 of rat bSV2C (**Supplementary Fig. 2**), which are not observed in the structure of the
76 human bSV2C-H_CA complex probably due to the different crystal packing modes¹¹.
77 Interestingly, R1294 only exists in two of the eight BoNT/A subtypes currently known
78 (BoNT/A1 and A4). Second, a cation- π stacking interaction between BoNT/A1-R1156—
79 exclusively existing in subtype BoNT/A1—and human SV2C-F563, previously thought to be
80 critical for BoNT/A1-SV2C recognition¹¹, does not exist in the rat bSV2C-H_CA complex

81 because rat SV2C has a leucine (L563) in the place of human SV2C-F563. Leucine is also the
82 homologous residue on SV2A and SV2B in both humans and rodents (**Supplementary Fig. 1c**).
83 These findings suggest that the side-chain mediated interactions may vary significantly among
84 different BoNT/A subtypes and SV2 isoforms, thus unlikely provide sufficient binding
85 specificity and affinity between them. Therefore, some crucial BoNT/A1-SV2 interactions are
86 missing in the crystal structures of HcA-bSV2C complexes described here and previously ¹¹.

87

88 **SV2 glycosylation is crucial for BoNT/A1 binding to neurons**

89 Native SV2s are glycosylated in neurons ¹⁴, and one of the three N-linked glycosylation motifs in
90 L4—conserved in all SV2 isoforms across vertebrates—is located at the center of the BoNT/A1-
91 binding interface of SV2 (e.g. N573 in SV2A, N516 in SV2B, and N559 in SV2C for human)
92 (**Supplementary Fig. 1c**). To explore the functional role of this N-linked glycan, we utilized a
93 molecule replacement approach to express either wild type (WT) SV2A-C, or the corresponding
94 deglycosylation mutants (SV2A-N573A, SV2B-N516A, and SV2C-N559A) in
95 hippocampal/cortical neurons cultured from SV2A/SV2B double knockout (KO) mice. Most
96 hippocampal/cortical neurons do not express SV2C ¹⁴, and thus these neurons cultured from
97 SV2A/SV2B double KO mice serve as a SV2-null neuron model. These deglycosylation
98 mutations of SV2 do not affect protein-protein interactions with BoNT/A1, as e.g. bSV2C-
99 N559A maintained a WT-like binding to HcA ¹¹.

100 The deglycosylation mutants of SV2A, 2B, and 2C all showed a lower molecular weight
101 compared to WT SV2s, confirming that this Asn residue is indeed glycosylated in neurons (**Fig.**
102 **1 and Supplementary Fig. 3**). The expression level of SV2A-N573A was comparable to the
103 WT SV2A, but there is a drastic reduction of SV2B-N516A expression and a mild reduction of
104 SV2C-N559A expression (**Supplementary Fig. 3**). It suggests that glycosylation at this site is
105 crucial for folding and/or stability of SV2B and to a lesser degree for SV2C—a known function
106 of N-linked glycans ¹⁵.

107 We thus focused on SV2A-N573A and SV2C-N559A, and examined SV2-mediated toxin entry
108 for BoNT/A1 and BoNT/D by analyzing the cleavage of synaptosomal-associated protein of 25
109 kDa (SNAP-25, the substrate of BoNT/A1) and synaptobrevin/vesicle-associated membrane
110 protein 2 (VAMP2, the substrate of BoNT/D) after toxin exposure. BoNT/D serves here as an
111 internal control for regular trafficking and sorting of SV2 mutants, as BoNT/D uses SV2s as
112 receptors independent to N-glycosylation ⁸. Furthermore, we have previously shown that
113 BoNT/B1 that does not use SV2 as its receptor binds and enters the WT and SV2 KO neurons at
114 similar levels ^{5,7}. We found that the SV2 KO neurons did not show BoNT/A1 entry at the
115 conditions tested, which is likely due to BoNT/A1's low affinity for the ganglioside receptor that
116 is unable to allow cell entry in the absence of SV2 ^{16,17}. Expression of SV2A-N573A and SV2C-
117 N559A mediated significantly less entry of BoNT/A1 compared to the WT SV2s, whereas
118 BoNT/D entry was not affected (**Fig. 1**). These results suggest that SV2 glycosylation at this
119 strictly conserved site clearly contributes to BoNT/A1 binding and entry into neurons.

120

121 **The SV2C glycans significantly enhances HcA binding**

122 Glycosylation is a common and highly diverse post-translational protein modification that
123 profoundly alters the protein behavior ¹⁵. Do the N-glycans contribute directly to BoNT/A1

124 binding? In this regard, we first carried out surface plasmon resonance (SPR) to examine how
125 HcA binds to the human bSV2C. We found that the binding displays a fast association rate (k_a :
126 $1.5 \times 10^6 \text{ M}^{-1}\text{s}^{-1}$) and a fast dissociation rate (k_d : 0.11 s^{-1}) (**Fig. 2a**), and the overall dissociation
127 constant (K_D) of $\sim 86 \text{ nM}$ was comparable to a previously reported K_D of 260 nM determined by
128 fluorescence anisotropy experiment¹¹. The nature of this transient interaction is consistent with
129 the pattern of backbone-to-backbone interactions revealed in the crystal structure, but difficult to
130 reconcile with the extreme specificity of BoNT/A1 toward neurons.

131 We then expressed the human SV2C-L4 (residues V473-T567) as a secreted protein using
132 human embryonic kidney 293 cells (HEK293), to mimic the physiologically relevant
133 glycosylated receptor. HEK293 cells have been widely used to produce glycoproteins with
134 human glycosylation patterns¹⁸. The resulting protein (referred to as gSV2C, g stands for
135 glycosylation) is glycosylated as evidenced by the appearance of multiple bands on SDS-PAGE
136 that are bigger than its peptide mass and represent heterogeneous glycoforms. We characterized
137 binding of HcA to gSV2C by SPR, which revealed two binding components (**Fig. 2b-c and**
138 **Supplementary Fig. 4**). A transient low affinity binding ($K_D \sim 220 \text{ nM}$) closely resembles the
139 binding of HcA to bSV2C, which is likely due to heterogeneous glycosylation of SV2C under
140 over-expression conditions¹⁹. Notably, a high affinity binding ($K_D \sim 15 \text{ nM}$) of gSV2C displays a
141 ~ 22 -fold slower dissociation rate and a ~ 4 -fold slower association rate compared to bSV2C. The
142 slightly decreased association rate of gSV2C likely stems from restricted carbohydrate flexibility
143 upon toxin binding, a physiological event that BoNT/A1 will encounter *in vivo* because the
144 neuronal SV2s are glycosylated. Therefore, the relatively fast association rate displayed by
145 bSV2C artificially increases the binding affinity of bSV2C. Taken together, these data
146 demonstrate that the glycans of gSV2C stabilize the HcA-gSV2C complex by significantly
147 decreasing the dissociation rate.

148

149 **The crystal structure of HcA in complex with the glycosylated human SV2C**

150 We next determined the crystal structure of HcA in complex with gSV2C at 2.0 \AA resolution
151 (**Table 1**). The overall architecture of the HcA-gSV2C complex is similar to that of the bSV2C
152 complex (RMSD $\sim 0.88 \text{ \AA}$ over 489 aligned Ca pairs). A complex-type N-linked glycan attached
153 to gSV2C-N559 was observed with clear electron densities for the quadruple-saccharide core
154 made up of two N-acetylglucosamine (NAG), a mannose (BMA), and a fucose (FUC) (**Fig. 3**
155 **and Supplementary Fig. 5**). There are two other putative N-linked glycosylation sites (N484
156 and N534) that are localized on SV2C-L4 and also conserved on SV2A and SV2B
157 (**Supplementary Fig. 1c**). Only one NAG could be resolved in the electron density for the N534
158 glycan likely due to its high mobility, whereas no sugar could be identified at N484. SV2C N484
159 and N534 are located far away from BoNT/A1-binding interface, and thus unlikely to directly
160 participate in toxin binding.

161 Remarkably the N559-glycan directly interacts with HcA through a network of hydrogen bonds
162 and van der Waals contacts. The most prominent are stacking interactions between residues F953
163 and H1064 of HcA and the hydrophobic faces of the two NAG. In addition, ten well-defined
164 water molecules act as a molecular “glue” in the glycan-HcA interface to further strengthen the
165 interactions (**Fig. 3d-e and Supplementary Table 1**). These interactions almost double the
166 contact area between HcA and SV2C from 557 to 925 \AA^2 . There are also weak electron densities
167 beyond the mannose, suggesting that there might be more extensive HcA-glycan interactions that

168 were not resolved, possibly due to the inherent flexibility of glycans and heterogeneous
169 glycosylation. This structure unambiguously reveals that the N559-glycan of SV2C is recognized
170 directly by BoNT/A1 as an integral part of the toxin-binding site.

171

172 **BoNT/A1-glycan binding is conserved across SV2 isoforms and is critical for BoNT/A1** 173 **binding to neurons**

174 We then sought to understand the functional role of protein-glycan interactions in BoNT/A1-SV2
175 recognition. Based on the crystal structure, we designed a set of single-site mutations on H_CA
176 that selectively disrupt glycan binding: F953G and H1064G abolish the critical stacking of
177 aromatic side chains against the sugar rings, and F953R, H1064R, G1292Q, and G1292R cause
178 clashes between their bulky side chains and the N559-glycan. None of these mutations affected
179 H_CA folding and stability as verified by thermal denaturation experiments, nor did they affect
180 H_CA binding to bSV2C based on pull-down and SPR studies. As expected, these mutants
181 markedly decreased H_CA binding to gSV2C, strongly supporting the direct involvement of
182 N559-glycan of SV2C in BoNT/A1 binding (**Supplementary Figs. 6 and 7a-c**). Interestingly,
183 SPR studies showed that the glycan-binding deficient H_CA-F953G binds to gSV2C much weaker
184 than bSV2C (K_D : ~760 nM vs. ~160 nM) (**Supplementary Fig. 7d-f**). Therefore, the native
185 neuronal SV2s that are always glycosylated initially impose steric hindrances for BoNT/A1
186 recognition. But BoNT/A1 manages to overcome this obstacle by directly employing SV2
187 glycans to strengthen binding.

188 We examined how these H_CA mutants bind to native SV2s in neurons. First, we analyzed
189 binding of H_CA to endogenous SV2A and SV2B using cultured rat hippocampal/cortical neuron
190 ¹⁴ (**Fig. 4a-b**). Mutations F953G, F953R, G1292Q, and G1292R largely abolished binding of
191 H_CA to neurons; H1064G and H1064R also drastically reduced binding, suggesting that protein-
192 glycan interactions are essential for BoNT/A1 binding to native SV2s on neurons. We further
193 examined neurons that exclusively expressed SV2A, 2B, or 2C: hippocampal/cortical neurons
194 cultured from SV2A(+/+)SV2B(-/-) mice served as neurons that only express SV2A, and
195 neurons that only express SV2B or SV2C were created by infecting neurons cultured from
196 SV2A(-/-)SV2B(-/-) mice with lentiviruses that express SV2B or SV2C, respectively. Mutating
197 glycan-binding residues on H_CA (e.g. F953G, G1292R, and H1064G) reduced H_CA binding in
198 all cases tested, demonstrating that BoNT/A1-glycan interactions are conserved and essential for
199 all three SV2 isoforms (**Fig. 4c-e and Supplementary Fig. 8**).

200

201 **The conserved SV2 N-glycan allows to tolerate genetic changes on various BoNT/A** 202 **subtypes**

203 Complementing our studies on protein-glycan interactions, we also examine the contribution of
204 side-chain-mediated protein-protein interactions to SV2 recognition that could vary significantly
205 among the eight different BoNT/A subtypes (**Supplementary Fig. 9**). In this regard, residues
206 R1156 and R1294 of BoNT/A1 were mutated to their counterparts in other BoNT/A subtypes
207 (e.g. R1156E and R1294S), which disrupt their interactions with the peptide moiety of SV2C but
208 without affecting glycan binding. We used the double mutant H_CA-T1145A-T1146A as a control
209 ¹¹. These two Thr residues, located at the core of protein-protein interface, are conserved in all
210 BoNT/A subtypes (**Supplementary Fig. 9**). We found that binding of H_CA-T1145A-T1146A to

211 cultured rat hippocampal/cortical neurons was abolished (**Fig. 4a-b**). This is consistent with an
212 earlier study showing that H_CA-T1145A-T1146A can no longer bind to bSV2C¹¹. Interestingly,
213 we found that H_CA-R1156E and R1294S still bound significantly to neurons (**Fig. 4a-b**), even
214 though they showed decreased binding to both human bSV2C and gSV2C *in vitro*
215 (**Supplementary Fig. 7**). These data suggest that loss of side-chain-mediated interactions at
216 R1156 and R1294 of BoNT/A1 is tolerated on neuronal surfaces likely due to the presence of
217 SV2 glycan and co-receptor gangliosides.

218

219 **SV2 glycan-binding is essential for the extreme potency of BoNT/A1 at motor nerve** 220 **terminals**

221 To further establish the physiological relevance of protein-glycan interactions, we produced full-
222 length BoNT/A1 containing single-site glycan-binding deficient mutations (F953G, F953R,
223 H1064G, H1064R, G1292V, or G1292R) and examined their neurotoxicity at motor nerve
224 terminals using an *ex vivo* mouse phrenic nerve hemi-diaphragm (MPN) assay (**Fig. 5**)²⁰.
225 Remarkably, all these mutations drastically reduced the potency of BoNT/A1. BoNT/A1-F953R
226 had no detectable toxicity even at the maximal concentration tested (200 nM), which reflects a
227 larger than 10⁶-fold of toxicity reduction even though it displayed fully functional Zn²⁺-
228 endoprotease activity *in vitro*. Mutation G1292R also severely reduced the toxicity by 350-fold
229²¹. Mutations H1064G and H1064R displayed 3- and 7-fold reduction, respectively. These data
230 demonstrate that glycan-binding is essential for the extreme potency of BoNT/A1 at the motor
231 nerve terminals, its physiological site of action.

232

233 **The SV2 glycan-binding mode is conserved in the newly identified BoNT/HA**

234 We next examined whether glycan binding is conserved in natural variants of BoNT/A1, as
235 BoNT genes are actively evolved and at least 40 different subtypes of BoNT have been reported
236¹. In this regard, we focused on a newly reported mosaic toxin type HA (BoNT/HA, also known
237 as BoNT/FA), which has a hybrid-like structure including a BoNT/A1-like H_C 22-26. H_CHA is
238 highly similar to H_CA (~83% identical) (**Supplementary Fig. 9**). Sequence alignment revealed
239 that most of the glycan-binding residues, such as F953 and H1064, are conserved in H_CA and
240 H_CHA, but residues R1156 and R1294 of H_CA are changed to M1148 and S1286 in H_CHA.
241 H_CHA showed much weaker binding to human bSV2C as compared to H_CA, whereas its binding
242 to human gSV2C was comparable to that of H_CA (**Fig. 6a**). It suggests that the loss of side-chain
243 interactions due to genetic changes of M1148 and S1286 in H_CHA is compensated by SV2C
244 glycan. In contrast, H_CHA-F943G (equivalent to H_CA-F953G) failed to bind to gSV2C based on
245 a pull-down assay, nor did it bind to cortical neurons, likely due to the disruption of glycan
246 binding (**Fig. 6a-b**). These data confirm that a similar glycan-binding mode is conserved in
247 H_CHA and is critical for its binding to SV2s on neurons.

248 Furthermore, we found that the SV2 glycan-binding residues are largely conserved in seven out
249 of the eight BoNT/A subtypes (BoNT/A1-A3 and A5-A8) that have been identified up to date
250 (**Supplementary Fig. 9**)²⁷. Notably, BoNT/A4 is the only one that has an Arg residue (R1292)
251 at the equivalent position of BoNT/A1-G1292. Since BoNT/A1-G1292R mutant drastically
252 decreases BoNT/A1 toxicity by blocking its binding to SV2 glycan (**Figs. 4-5 and**
253 **Supplementary Figs. 7-8**)²¹, we suggest that this is a major reason that causes the ~1,000-fold

254 reduced biological activity of BoNT/A4 compared to BoNT/A1²⁸. Taken together, our findings
255 suggest that BoNT/A1 and variants utilizes the genetically invariable carbohydrates as surrogate
256 amino acids to engage the host receptors. Synergistic binding to two distinct cell surface
257 receptors, SV2 (including its peptide and glycan moieties) and ganglioside, provides a plausible
258 explanation for the extreme potency of BoNT/A and its remarkable specificity for nerve
259 terminals (**Fig. 6c**).

260

261 **A new strategy for developing therapeutic antibodies against BoNT/A**

262 The novel glycan receptor for BoNT/A presents a promising target for developing toxin
263 inhibitors. Remarkably, we found that a BoNT/A1-neutralizing human monoclonal antibody
264 family CR2/CR1, which is currently in clinical trial^{29,30}, directly targets the glycan-binding site
265 on HcA with its first antigen-binding loop of the light chain variable region occupying the
266 glycan-binding site (**Fig. 7a**). The key epitopes for CR2/CR1 include precisely residues F953
267 and H1064²⁹. Interestingly, residue F36 of CR2/CR1 uses a π -stacking interaction to bind
268 BoNT/A1-H1064, mimicking its interactions with SV2C N559-glycan. CR2/CR1 also blocks
269 binding of BoNT/A1 to bSV2C²¹, but this is due to the large size of CR2/CR1 causing side-to-
270 side clash with bSV2C, as CR2/CR1 and bSV2C have non-overlapping binding sites on HcA
271 (**Fig. 7b-d**). Together our data reveal that the strong neutralization potency of CR2/CR1 is
272 empowered by simultaneously blocking BoNT/A1 binding to the glycan and peptide moieties of
273 SV2.

274

275 **DISCUSSION**

276 Host cell-surface glycans are crucial for pathogen recognition. For example, influenza
277 hemagglutinins use carbohydrates in determining the host range (e.g. swine, avian or human)³¹.
278 Our results reveal a novel host-recognition strategy, by which pathogens simultaneously
279 recognize a protein segment and the neighboring glycans as a composite binding site. This
280 unique strategy uses a conserved post-translational modification as an evolutionarily static
281 recognition site, in addition to protein-protein interactions that encode the location and
282 specificity information. Together, it provides a powerful solution to address the competing needs
283 of achieving highly specific binding while also tolerating residue changes in receptors across
284 multiple isoforms and species variants.

285 Intriguingly, a similar strategy may be utilized by some important broad-neutralizing human
286 antibodies, which are capable of neutralizing multiple serotypes of targeted viruses, such as
287 dengue viruses and immunodeficiency virus-1 (HIV-1), by simultaneously recognizing the
288 protein components and the highly conserved glycans on virus proteins³²⁻³⁴. A similar model
289 was also recently demonstrated for Notch1 receptor binding with its ligand Delta like 4 (DLL4)
290³⁵, where DLL4 binds to the fucose and glucose at the base of an O-glycosylation site located
291 within the protein-protein interface. Therefore, our findings offer an important strategy for
292 engineering ligand-receptor interactions and broadly neutralizing antibodies for therapeutic
293 applications.

294

295 **Accession codes.** Atomic coordinates and structure factors for the HcA-bSV2C and HcA-gSV2C
296 complexes will be deposited in the Protein Data Bank.

298 ACKNOWLEDGEMENTS

299 This work was partly supported by National Institute of Allergy and Infectious Diseases (NIAID)
300 grants R01AI091823 and R21AI123920 to R.J. and R01AI096169 to M.K.; by National Institute
301 of Neurological Disorders and Stroke (NINDS) Grant R01NS080833 to M.D.; and by the
302 Bundesministerium für Bildung und Forschung grants FK031A212A to A.R. and FK031A212B
303 to Brigitte G. Dorner (RKI). NE-CAT at the Advanced Photon Source (APS) is supported by a
304 grant from the National Institute of General Medical Sciences (P41 GM103403). The Pilatus 6M
305 detector on 24-ID-C beam line is funded by a NIH-ORIP HEI grant (S10 RR029205). Use of the
306 APS, an Office of Science User Facility operated for the U.S. Department of Energy (DOE)
307 Office of Science by Argonne National Laboratory, was supported by the U.S. DOE under
308 Contract No. DE-AC02-06CH11357.

309

310 AUTHOR CONTRIBUTIONS

311 G.Y. and S.M. performed the cloning and mutagenesis. G.Y., K.L. and R.J. carried out the
312 protein expression, purification, characterization and crystallographic studies. K.P. collected the
313 X-ray diffraction data. S.Z. and M.D. performed all experiments on cultured neurons. A.R. and
314 S.M. generated the full-length BoNT/A1 mutants and performed the MPN assay with support of
315 Nadja Krez. Dr. Jasmin Weisemann cloned HcHA. D.S., K.B. and M.K. performed the SPR
316 studies. R.J., M.D. and A.R. wrote the manuscript with input from other authors.

317

318 COMPETING FINANCIAL INTERESTS

319 The authors declare no competing financial interests.

320

321

322 REFERENCES

323

- 324 1. Rossetto, O., Pirazzini, M. & Montecucco, C. Botulinum neurotoxins: genetic, structural
325 and mechanistic insights. *Nat Rev Microbiol* **12**, 535-49 (2014).
- 326 2. Montecucco, C. How do tetanus and botulinum neurotoxins bind to neuronal
327 membranes? *Trends Biochem Sci* **11**, 314-17 (1986).
- 328 3. Montecucco, C., Rossetto, O. & Schiavo, G. Presynaptic receptor arrays for clostridial
329 neurotoxins. *Trends Microbiol* **12**, 442-6 (2004).
- 330 4. Rummel, A. Double Receptor Anchorage of Botulinum Neurotoxins Accounts for their
331 Exquisite Neurospecificity. *Curr Top Microbiol Immunol* **364**, 61-90 (2013).
- 332 5. Dong, M. et al. SV2 is the protein receptor for botulinum neurotoxin A. *Science* **312**,
333 592-6 (2006).
- 334 6. Mahrhold, S., Rummel, A., Bigalke, H., Davletov, B. & Binz, T. The synaptic vesicle
335 protein 2C mediates the uptake of botulinum neurotoxin A into phrenic nerves. *FEBS Lett* **580**,
336 2011-4 (2006).
- 337 7. Dong, M. et al. Glycosylated SV2A and SV2B mediate the entry of botulinum neurotoxin
338 E into neurons. *Mol Biol Cell* **19**, 5226-37 (2008).
- 339 8. Peng, L., Tepp, W.H., Johnson, E.A. & Dong, M. Botulinum neurotoxin D uses synaptic
340 vesicle protein SV2 and gangliosides as receptors. *PLoS Pathog* **7**, e1002008 (2011).

- 341 9. Rummel, A. et al. Botulinum neurotoxins C, E and F bind gangliosides via a conserved
342 binding site prior to stimulation-dependent uptake with botulinum neurotoxin F utilising the
343 three isoforms of SV2 as second receptor. *J Neurochem* **110**, 1942-54 (2009).
- 344 10. Fu, Z., Chen, C., Barbieri, J.T., Kim, J.J. & Baldwin, M.R. Glycosylated SV2 and
345 gangliosides as dual receptors for botulinum neurotoxin serotype F. *Biochemistry* **48**, 5631-41
346 (2009).
- 347 11. Benoit, R.M. et al. Structural basis for recognition of synaptic vesicle protein 2C by
348 botulinum neurotoxin A. *Nature* **505**, 108-11 (2014).
- 349 12. Chai, Q. et al. Structural basis of cell surface receptor recognition by botulinum
350 neurotoxin B. *Nature* **444**, 1096-100 (2006).
- 351 13. Jin, R., Rummel, A., Binz, T. & Brunger, A.T. Botulinum neurotoxin B recognizes its
352 protein receptor with high affinity and specificity. *Nature* **444**, 1092-5 (2006).
- 353 14. Janz, R. & Sudhof, T.C. SV2C is a synaptic vesicle protein with an unusually restricted
354 localization: anatomy of a synaptic vesicle protein family. *Neuroscience* **94**, 1279-90 (1999).
- 355 15. Helenius, A. & Aebi, M. Intracellular functions of N-linked glycans. *Science* **291**, 2364-9
356 (2001).
- 357 16. Rummel, A., Mahrhold, S., Bigalke, H. & Binz, T. The HCC-domain of botulinum
358 neurotoxins A and B exhibits a singular ganglioside binding site displaying serotype specific
359 carbohydrate interaction. *Mol Microbiol* **51**, 631-43 (2004).
- 360 17. Pirazzini, M., Rossetto, O., Bolognese, P., Shone, C.C. & Montecucco, C. Double
361 anchorage to the membrane and intact inter-chain disulfide bond are required for the low pH
362 induced entry of tetanus and botulinum neurotoxins into neurons. *Cell Microbiol* **13**, 1731-43
363 (2011).
- 364 18. Swiech, K., Picanco-Castro, V. & Covas, D.T. Human cells: new platform for
365 recombinant therapeutic protein production. *Protein Expr Purif* **84**, 147-53 (2012).
- 366 19. Croset, A. et al. Differences in the glycosylation of recombinant proteins expressed in
367 HEK and CHO cells. *J Biotechnol* **161**, 336-48 (2012).
- 368 20. Bigalke, H. & Rummel, A. Botulinum Neurotoxins: Qualitative and Quantitative
369 Analysis Using the Mouse Phrenic Nerve Hemidiaphragm Assay (MPN). *Toxins (Basel)* **7**, 4895-
370 905 (2015).
- 371 21. Strotmeier, J. et al. Identification of the synaptic vesicle glycoprotein 2 receptor binding
372 site in botulinum neurotoxin A. *FEBS Lett* **588**, 1087-93 (2014).
- 373 22. Barash, J.R. & Arnon, S.S. A novel strain of Clostridium botulinum that produces type B
374 and type H botulinum toxins. *J Infect Dis* **209**, 183-91 (2014).
- 375 23. Gonzalez-Escalona, N. et al. Draft Genome Sequence of Bivalent Clostridium botulinum
376 Strain IBCA10-7060, Encoding Botulinum Neurotoxin B and a New FA Mosaic Type. *Genome*
377 *Announc* **2**(2014).
- 378 24. Kalb, S.R. et al. Functional characterization of botulinum neurotoxin serotype H as a
379 hybrid of known serotypes F and A (BoNT F/A). *Anal Chem* **87**, 3911-7 (2015).
- 380 25. Maslanka, S.E. et al. A Novel Botulinum Toxin, Previously Reported as Serotype H, has
381 a Hybrid Structure of Known Serotypes A and F that is Neutralized with Serotype A Antitoxin. *J*
382 *Infect Dis* (2015).
- 383 26. Fan, Y. et al. Immunological Characterization and Neutralizing Ability of Monoclonal
384 Antibodies Directed Against Botulinum Neurotoxin Type H. *J Infect Dis* (2016).
- 385 27. Kull, S. et al. Isolation and functional characterization of the novel Clostridium
386 botulinum neurotoxin A8 subtype. *PLoS One* **10**, e0116381 (2015).

387 28. Whitemarsh, R.C. et al. Characterization of botulinum neurotoxin A subtypes 1 through 5
388 by investigation of activities in mice, in neuronal cell cultures, and in vitro. *Infect Immun* **81**,
389 3894-902 (2013).

390 29. Garcia-Rodriguez, C. et al. Molecular evolution of antibody cross-reactivity for two
391 subtypes of type A botulinum neurotoxin. *Nat Biotechnol* **25**, 107-16 (2007).

392 30. Nayak, S.U. et al. Safety and pharmacokinetics of XOMA 3AB, a novel mixture of three
393 monoclonal antibodies against botulinum toxin A. *Antimicrob Agents Chemother* **58**, 5047-53
394 (2014).

395 31. Skehel, J.J. & Wiley, D.C. Receptor binding and membrane fusion in virus entry: the
396 influenza hemagglutinin. *Annu Rev Biochem* **69**, 531-69 (2000).

397 32. Rouvinski, A. et al. Recognition determinants of broadly neutralizing human antibodies
398 against dengue viruses. *Nature* (2015).

399 33. Garces, F. et al. Structural evolution of glycan recognition by a family of potent HIV
400 antibodies. *Cell* **159**, 69-79 (2014).

401 34. Kong, L. et al. Supersite of immune vulnerability on the glycosylated face of HIV-1
402 envelope glycoprotein gp120. *Nat Struct Mol Biol* **20**, 796-803 (2013).

403 35. Luca, V.C. et al. Structural biology. Structural basis for Notch1 engagement of Delta-like
404 4. *Science* **347**, 847-53 (2015).

405 36. Laskowski, R.A. & Swindells, M.B. LigPlot+: multiple ligand-protein interaction
406 diagrams for drug discovery. *J Chem Inf Model* **51**, 2778-86 (2011).

407 37. Stenmark, P., Dupuy, J., Imamura, A., Kiso, M. & Stevens, R.C. Crystal structure of
408 botulinum neurotoxin type A in complex with the cell surface co-receptor GT1b-insight into the
409 toxin-neuron interaction. *PLoS Pathog* **4**, e1000129 (2008).

410 38. Matsumiya, S. et al. Structural comparison of fucosylated and nonfucosylated Fc
411 fragments of human immunoglobulin G1. *J Mol Biol* **368**, 767-79 (2007).

412

413 **FIGURE LEGENDS**

414

415 **Figure 1** SV2 glycosylation is critical for BoNT/A1 binding and entry into neurons. Lentivirus
416 was used to infect mouse SV2A(-/-)SV2B(-/-) neurons to create neurons that express either the
417 WT or the deglycosylation mutants of SV2A (**a**) or SV2C (**b**). Neurons were simultaneously
418 exposed to BoNT/A1 (1 nM) and BoNT/D (0.1 nM) in a high K⁺ buffer for 5 minutes at 37°C.
419 Unbound toxin was washed away, and the intoxicated cells were incubated for another 8 hour.
420 Cell lysates were harvested and subjected to immunoblot analysis using mouse monoclonal
421 antibodies against SNAP-25 (Cl 71.2), VAMP2 (Cl 69.1), and SV2 (pan-SV2). BoNT/D served
422 as an internal control to confirm that SV2 mutants still sorted and localized correctly. Cleavage
423 of SNAP-25 by BoNT/A1 generates a smaller fragment that is marked by an asterisk. Actin
424 served as a loading control.

425 **Figure 2** Glycosylation in SV2 luminal domain enhances BoNT/A1 binding. (**a**) Sensorgrams of
426 H_CA binding to immobilized human bSV2C (blue) overlaid with a fit of 1:1 binding model
427 (black). Since equilibrium binding was reached for all conditions tested, a steady state affinity
428 was also determined (insert). (**b**) H_CA binding to immobilized human gSV2C (red) was best fit to
429 a heterogeneous binding model (black), whereas a 1:1 binding model was inapplicable
430 (**Supplementary Fig. 4**). Insert: individual contributions of the two binding events observed in
431 the heterogeneous interaction (blue and green). (**c**) Kinetic binding rates and affinities for H_CA
432 binding to human bSV2C or gSV2C. Shown values represent the mean ± S.D. (n = 2 for bSV2C,
433 n = 3 for gSV2C).

434 **Figure 3** Structure of H_CA in complex with human gSV2C. (**a**) Cartoon representation of the
435 complex whereas H_CA is gold and gSV2C is green. The black oval highlights the interacting β-
436 strands between them. gSV2C-N559 and the attached N-linked glycan are shown in the stick
437 models. (**b**) A ~150° rotation of the complex about a vertical axis. (**c-d**) Close-up views of the
438 protein-protein and protein-glycan association interfaces between H_CA and gSV2C. H_CA is in
439 surface representation (gold), whereas H_CA residues that directly interact with the peptide moiety
440 of gSV2C or the N559 glycan are colored purple and light blue, respectively. Well-defined water
441 molecules that mediate H_CA-glycan binding are shown as green spheres. (**e**) Extensive
442 interactions between gSV2C-N559 glycan and H_CA. A schematic representation of the glycan
443 structure is shown. The plots were generated using LIGPLOT³⁶. H_CA and gSV2C residues are
444 labeled brown and green, respectively. Hydrogen bonds are indicated by dashed green lines. Key
445 hydrogen bonding distances are listed in **Supplementary Table 1**. Residues involved in
446 hydrophobic interactions are represented by an arc with spokes radiating towards the binding
447 partners they contact.

448 **Figure 4** Site-directed mutagenesis analysis of the SV2-binding site on H_CA. (**a-b**) Binding of
449 H_CA variants (100 nM, 5 min, 37°C in a high K⁺ buffer) to rat hippocampal/cortical neurons was
450 analyzed by immunostaining (panel a) or immunoblot (panel b). Scale bar, 20 μm.
451 Synaptophysin (Syp) served as a loading control. (**c-e**) Binding of H_CA variants (100 nM, 5 min)
452 to neurons that express individual SV2A, 2B, or 2C was analyzed by immunoblot.
453 Hippocampal/cortical neurons cultured from SV2A(+/+)SV2B(-/-) mice served as neurons that
454 only express SV2A (panel c). Neurons that only express SV2B or SV2C were created by
455 infecting neurons cultured from SV2A(-/-)SV2B(-/-) mice with lentiviruses that express SV2B

456 (panel d) or SV2C (panel e). The results of immunostaining analysis are shown in
457 **Supplementary Fig. 8.**

458
459 **Figure 5** Glycan binding-deficient BoNT/A1 displays drastic decreased neurotoxicity as
460 examined by the mouse phrenic nerve (MPN) assay. BoNT/A1 F953R mutant showed no
461 detectable toxicity even at the maximal concentration tested (200 nM), indicating a larger than
462 10^6 -fold reduction on toxicity. Shown are mean \pm S.D. of 3-6 technical replicates.

463 **Figure 6** The SV2 glycan binding mode is conserved in BoNT/HA. **(a)** The SV2C glycan plays
464 an indispensable role for H_CHA binding as demonstrated by a pull-down assay using human
465 bSV2C (with a SUMO tag) or gSV2C as baits. “Mu” is H_CHA-F943G mutant. **(b)** The F943G
466 mutation dramatically decreased H_CHA binding to rat cortical neurons as analyzed by
467 immunostaining and immunoblot. **(c)** Proposed model for simultaneous binding of BoNT/A1 to
468 two neuronal surface receptors: glycosylated SV2 and ganglioside. GT1b is modeled based on
469 the structure of a GT1b-bound H_CA (PDB code 2VU9)³⁷. A representative complex type N-
470 linked glycan is modeled based on the structure of a glycan of human IgG1 (PDB code 3AVE)
471 ³⁸. The glycan core that is observed in the H_CA-gSV2C complex is colored green, whereas the
472 remaining carbohydrates (mannose and NAG colored gray) could potentially extend to the N-
473 terminal sub-domain of H_CA (H_{CNA}).

474 **Figure 7** The SV2 glycan-binding site on BoNT/A1 is the target for the neutralizing antibody
475 CR1. **(a-b)** BoNT/A1-neutralizing therapeutic antibody CR1 (PDB code: 2NYY)²⁹ occupies the
476 SV2C glycan-binding site on H_CA, but does not affect H_CA’s SV2C peptide-binding site. An
477 arrow in the schematic diagram indicates the side-to-side clash between SV2C and CR1. **(c)** A
478 close-up view of the interface. gSV2C-N559 glycan (green), H_CA-F953 and -H1064 (gold),
479 residues 30-36 of CR1 ligand chain (LC, red), and residues 101-103 of CR1 heavy chain (HC,
480 gray) are shown in stick models. **(d)** Residues of H_CA that exclusively bind SV2C peptide, N559
481 glycan or CR1 are colored in purple, green or cyan, respectively, while the H_CA residues that are
482 contacted by both N559 glycan and CR1 are in blue.

483

Table 1 Data collection and refinement statistics.

	HcA-bSV2C (rat)	HcA-gSV2C (human)
Data collection		
Space group	P 1 21 1	C 1 2 1
Cell dimensions		
<i>a</i> , <i>b</i> , <i>c</i> (Å)	88.66, 143.99, 110.92	109.00, 111.85, 126.25
α , β , γ (°)	90, 93.6, 90	90, 101.3, 90
Resolution (Å)	87.76-2.64 (2.73-2.64)	123.8-2.0 (2.03-2.00)
<i>R</i> _{meas}	0.172 (1.454)	0.159 (0.889)
CC1/2	0.991 (0.599)	0.984 (0.722)
<i>I</i> / σ (<i>I</i>)	9.1 (1.4)	6.7 (2.1)
Completeness (%)	99.44 (99.20)	99.6 (99.9)
Redundancy	3.4 (3.1)	2.9 (2.9)
Refinement		
Resolution (Å)	87.76-2.64	123.81-2.00
No. reflections	80,958	99,659
<i>R</i> _{work} / <i>R</i> _{free}	0.239/0.271	0.176/0.216
No. atoms		
Protein	16,825	8,645
Ligand/ion	-	128
Water	162	659
B-factors		
Protein	58.50	44.50
Ligand/ion	-	58.70
Water	55.40	51.50
r.m.s. deviations		
Bond lengths (Å)	0.012	0.009
Bond angles (°)	1.22	1.01

485 Statistics for the highest-resolution shell are shown in parentheses.

487 **METHODS**

488 **Construct design and cloning.** The gene of H_CA (residues N872–L1296) was cloned into
489 expression vector pQE30 with an N-terminal 6xHis-tag and a PreScission protease cleavage site.
490 H_CHA (residues E860–L1286) was cloned into pGEX-4T-2 vector that has a thrombin cleavage
491 site following GST. The core region of human SV2C-L4 (residues V473–T567) was cloned into
492 two different vectors: pET28a vector for *E. coli* expression and a pcDNA vector for mammalian
493 cell expression. For *E. coli* expression, a 6xHis/SUMO (*Saccharomyces cerevisiae* Smt3p) tag
494 was introduced to the N-terminus of SV2C-L4 to facilitate protein expression and purification
495 (SUMO-bSV2C). For mammalian cell expression, a human IL2 signal sequence
496 (MYRMQLLSIALSLALVTNS), a 9xHis-tag, and a Factor Xa cleavage site were added to the
497 N-terminus of SV2C-L4 (gSV2C). A second SV2C mammalian expression construct was made
498 based on gSV2C by inserting SUMO between the Factor Xa site and SV2C (SUMO-gSV2C).
499 Rat SV2C-L4 (residues P455–Y577) was covalently linked to the C-terminus of H_CA through a
500 peptide linker composed of a thrombin cleavage site (LVPRGS) and a PreScission protease
501 cleavage site (LEVLFGQP). The covalently linked H_CA-rbSV2C was cloned into pET28a vector
502 with an N-terminal 6xHis-tag and a thrombin cleavage site. All H_CA and H_CHA mutations were
503 generated using QuikChange site-directed mutagenesis (Agilent). All pH6tBoNTA mutants were
504 prepared using the GeneTailor method (Invitrogen GmbH, Karlsruhe, Germany) employing
505 suitable primers and pH6tBoNTA as template DNA ²¹.

506 **Protein expression and purification.** H_CA, H_CHA, SUMO-bSV2C, and H_CA-rbSV2C were
507 expressed in *E. coli* strain BL21-Star (DE3) (Invitrogen). Bacteria were cultured at 37°C in LB
508 medium containing appropriate selecting antibiotics. The temperature was reduced to 18°C when
509 OD₆₀₀ reached 0.4. Expression was induced with 0.2 mM IPTG (isopropyl-b-D-
510 thiogalactopyranoside) when OD₆₀₀ reached 0.7, and continued at 18°C for ~16 hours. The cells
511 were harvested by centrifugation and stored at -80°C until use.

512 Wild-type and mutated recombinant full-length neurotoxin H6tBoNTA were produced under
513 biosafety level 2 containment (project number GAA A/Z 40654/3/123) utilizing the *E. coli* strain
514 M15pREP4 (Qiagen, Hilden, Germany) during 16 h of induction at 22°C in the presence of 0.2
515 mM IPTG, and were purified on Co²⁺-Talon matrix (Takara Bio Europe S.A.S., France). Full-
516 length neurotoxins were eluted using 50 mM Tris-HCl, pH 8.0, 150 mM NaCl, and 250 mM
517 imidazole, subjected to size-exclusion chromatography (SEC; Superdex-200 16/60 column, GE
518 Healthcare, Germany) in 100 mM Tris-HCl, pH 8.0, and 150 mM NaCl, frozen in liquid nitrogen
519 and kept at -70°C.

520 The His-tagged proteins (H_CA, SUMO-bSV2C and H_CA-rbSV2C) were purified using Ni²⁺-NTA
521 (nitrilotriacetic acid, Qiagen, Hilden, Germany) affinity resins in a buffer containing 50 mM
522 Tris, pH 8.0, 400 mM NaCl, and 40 mM imidazole. The proteins were eluted with a high-
523 imidazole buffer (50 mM Tris, pH 8.0, 400 mM NaCl, and 300 mM imidazole) and then dialyzed
524 at 4°C against a buffer containing 20 mM HEPES, pH 7.5, and 150 mM NaCl. The His-tag of
525 H_CA and the His/SUMO-tag of SUMO-bSV2C were cleaved by PreScission and SUMO
526 proteases, respectively. For the covalently linked H_CA-rbSV2C, both thrombin and PreScission
527 protease were used to cut the linker between the two proteins in order to avoid potential
528 conformational constraint. GST-H_CHA fusion protein was purified using glutathione Sepharose

529 4B affinity resin (GE Healthcare) in a buffer containing 20 mM HEPES, pH 7.5, and 150 mM
530 NaCl. H_CHA was then released from the resins by on-column cleavage using thrombin.

531 Tag-cleaved H_CA and H_CHA were further purified by MonoS ion-exchange chromatography
532 (GE Healthcare) in a buffer containing 50 mM MES, pH 6.0, and eluted with a NaCl gradient.
533 The peak fractions were then subjected to Superdex-200 SEC (GE Healthcare) in a buffer
534 containing 20 mM sodium phosphate, pH 6.0, and 50 mM NaCl. SUMO-bSV2C (His/SUMO-tag
535 cleaved or un-cleaved) and the cleaved H_CA-rbSV2C were further purified by Superdex-200
536 SEC in a buffer containing 20 mM HEPES, pH 7.5, and 150 mM NaCl. H_CA-rbSV2C was
537 concentrated to ~2 mg/ml for crystallization.

538 SUMO-gSV2C and gSV2C were expressed and secreted from HEK 293 cells (BioLegend) and
539 purified directly from cell culture media using Ni²⁺-NTA. The proteins were eluted from the
540 resins with high concentration of imidazole and dialyzed against a buffer containing 50 mM Tris,
541 pH 8.0, and 400 mM NaCl. gSV2C was then mixed with the purified H_CA at a molar ratio of
542 ~1:2, and the H_CA-gSV2C complex was isolated by Ni²⁺-NTA resins. After dialysis against a
543 buffer containing 20 mM HEPES, pH 7.5, and 150 mM NaCl, the complex was further purified
544 by Superdex-200 SEC using the same buffer. The complex was concentrated to ~10 mg/ml for
545 crystallization.

546 **Crystallization.** Initial crystallization screens were carried out using a Gryphon crystallization
547 robot (Art Robbins Instruments) with high-throughput crystallization screening kits (Hampton
548 Research and Qiagen). Extensive manual optimization was then performed at 20°C using the
549 hanging-drop vapor-diffusion method when proteins were mixed with reservoir solutions in 1:1
550 ratio. H_CA-rbSV2C was initially crystallized in a condition containing 100 mM sodium
551 cacodylate, pH 6.5, 13% polyethylene glycol (PEG) 3,350, and 200 mM NaCl. The best crystals
552 were obtained in the presence of 0.7% (v/v) 1-butanol, which was identified using an additive
553 screen kit (Hampton Research). The crystals were cryo-protected in the original mother liquor
554 supplemented with 20% (v/v) glycerol and flash-frozen in liquid nitrogen. The H_CA-gSV2C
555 complex was originally crystallized as thin plates in a condition composed of 100 mM sodium
556 acetate, pH 4.6, 20% PEG 3,350, and 200 mM ammonium phosphate monobasic. These crystals
557 diffracted poorly. After extensive additive screening and optimization, the best crystals were
558 obtained in the presence of 4% (w/v) polypropylene glycol P 400. The crystals were cryo-
559 protected in the reservoir solution supplemented with 20% (v/v) ethylene glycol and flash-frozen
560 in liquid nitrogen.

561 **Data collection and structure determination.** The X-ray diffraction data were collected at 100
562 K at the NE-CAT beamline 24-ID, Advanced Photon Source (APS). The data were processed
563 with XDS³⁹. The structure of H_CA-rbSV2C was determined by molecular replacement software
564 Phaser⁴⁰ using the structure of H_CA (PDB code 3FUO)¹⁰ as the search model. The structural
565 model of rbSV2C was manually built, and the structural modeling and refinement were carried
566 out iteratively using COOT⁴¹ and Refmac from the CCP4 suite⁴². This structure was later used
567 as the search model to determine the structure of the H_CA-gSV2C complex. All the refinement
568 progress was monitored with the free R value using a 5% randomly selected test set⁴³. The
569 structures were validated through the MolProbity web server⁴⁴ and showed excellent

570 stereochemistry. Data collection and structural refinement statistics are listed in Table 1. All
571 structure figures were prepared with PyMol (<http://www.pymol.org>).

572 **Pull-down assay.** The pull-down assay was performed using Ni²⁺-NTA resins in 1 ml buffer
573 containing 50 mM Tris, pH 8.0, 400 mM NaCl, 10 mM imidazole, and 0.1% Tween-20. SUMO-
574 bSV2C or gSV2C served as the bait while H_CA or H_CHA variants were the preys. SV2C was
575 pre-incubated with Ni²⁺-NTA resins at 4°C for 1 hour, and the unbound protein was washed
576 away. The resins were then divided into small aliquots (~ 5µg of bait) and mixed with the preys
577 (~ 30 µg). The pull-down assay was carried out at 4°C for ~1.5 hours. The resins were washed
578 twice, and the bound proteins were released from resins using 300 mM imidazole.

579 **Protein melting assay.** The thermal stability of H_CA or H_CHA variants was measured using a
580 fluorescence-based thermal shift assay on a StepOne real-time PCR machine (Life
581 Technologies). The protein (~5 µM) was mixed with the fluorescent dye SYPRO Orange
582 (Sigma-Aldrich) immediately before the experiment. The samples were heated from 25°C to
583 90°C in ~ 45 min. The midpoint of the protein-melting curve (T_m) was determined using the
584 analysis software provided by the instrument manufacturer. The data obtained from three
585 independent experiments were averaged to generate the bar graph.

586 **Surface plasmon resonance (SPR).** Binding kinetics and affinity were determined on a Biacore
587 X100 unit (GE Healthcare) at 25°C using HBS-EP+ (10 mM HEPES, pH 7.4, 150 mM NaCl, 3
588 mM EDTA, 0.05% Tween-20) as running buffer at a flow rate of 30 µL/min. Using standard
589 EDC/NHS amine coupling chemistry, SUMO-gSV2C or SUMO-bSV2C were coupled on flow
590 cell (Fc) 2 of a CM5 sensor chip (GE Healthcare) to a surface density of ~83 resonance units
591 (RUs) or ~105 RUs, respectively. Control Fc1 was blank immobilized by EDC/NHS activation
592 before blocking with 1 M ethanolamine (GE Healthcare).

593 For kinetic measurements, H_CA was injected in 1:3 dilution series ranging from 1,200 nM to
594 4.94 nM for gSV2C or 2,000 nM to 2.74 nM for bSV2C. Each measurement was started and
595 ended with injection of the highest analyte concentration to ensure retained binding capacity.
596 Association was monitored for 120 seconds by analyte injection followed by 300 second
597 injections of running buffer to monitor binding dissociation. Between measurements, the surface
598 was regenerated by 60 second injections of 10 mM glycine-HCl (pH 1.7) at 10 µL/min. Binding
599 kinetics were determined by fitting the double referenced⁴⁵ binding curves using the
600 heterogeneous (gSV2C) or the 1:1 Langmuir binding models (bSV2C) with global R_{max} and RI
601 set to zero (Biacore Evaluation Software 2.01). Due to the highly transient interaction of H_CA
602 with bSV2C, equilibrium binding was reached for all H_CA concentrations tested. Therefore,
603 steady state affinity was determined for bSV2C by fitting a four-parametric Hill equation to the
604 binding responses 65 seconds after analyte injection over log-transformed H_CA-concentrations
605 using Prism 5.04 (GraphPad) with bottom constraint set to zero. The good agreement between
606 the binding affinity determined by kinetic analysis and the steady state affinity proved that
607 kinetic binding rates for bSV2C were reliable despite being close to the measurement limits of
608 the instrument. Kinetic binding rates were determined by n = 2 (bSV2C) or n = 3 (gSV2C)
609 independent experiments. Shown values represent the mean ± standard deviation.

610 To compare the interaction of H_CA WT and its mutants with bSV2C (511 RUs) and separately
611 with gSV2C (479 RUs), the reactions were performed in the “interactive manual run mode”. The

612 HcA variants were injected at concentrations of 0.01, 1.0, 10, 25, 50, 75, 100 and 200 nM, each
613 in triplicate, and at a flow-rate of 10 μ L/min. The chip surface was regenerated by two injections
614 of glycine-HCl (10 mM, pH 2.0, 30 sec contact time) allowing the removal of the analyte
615 without changing the activity of the immobilized ligand. This was confirmed by the equal
616 responses obtained from the binding assays before and after regeneration. Results were plotted as
617 response (RU) versus concentration of HcA using Prism 6 (GraphPad Software Inc., La Jolla,
618 CA).

619 **Cell biology materials and constructs.** SV2A and SV2B knockout mice were obtained from the
620 Jackson Laboratory. Rat cDNAs encoding SV2A, SV2B, and SV2C were generously provided
621 by R. Janz (Houston, TX). They were cloned into a lentiviral vector (Lox-Syn-Syn) as we
622 previously described⁸. This vector contains two separate neuronal-specific synapsin promoters.
623 One promoter drives expression of SV2 and the other one drives expression of GFP as a marker.
624 Human cDNA encoding SV2C was obtained from PlasmID repository of Harvard Medical
625 School. Human monoclonal antibody against HcA (RAZ-1) was generously provided by J.
626 Marks (San Francisco, CA). Mouse monoclonal antibodies against VAMP2 (Cl 69.1), SNAP-25
627 (Cl 71.2), SV2 (pan-SV2), Syp (Cl 7.2) were generously provided by E. Chapman (Madison,
628 WI) and are available from Synaptic Systems (Göttingen, Germany). The following antibodies
629 were purchased from indicated vendors: mouse monoclonal antibody against actin (Sigma);
630 rabbit polyclonal antibody against synapsin (Millipore); rabbit polyclonal antibody against GFP
631 (Abcam). Purified BoNT/A1 of Hall-A strain and BoNT/D of D1873 strain were generously
632 provided by E. Johnson (Madison, WI).

633 **Neuron culture and lentivirus transduction.** Rat hippocampal/cortical neurons were prepared
634 from E18-19 embryos. Mouse SV2A/B double knockout neurons were prepared from postnatal
635 day 1 pups as previously described⁸. Dissected hippocampi and cortex were dissociated with
636 papain following manufacture instructions (Worthington Biochemical, NJ). Cells were plated on
637 poly-D-lysine coated coverslips. Experiments were carried out generally using DIV (days in
638 vitro) 13-15 neurons. Lentivirus were prepared as described previously using HEK293FT cells⁸.
639 Viruses were added to neurons at DIV5.

640 **HcA and HcHA binding to neurons.** Neurons were exposed to 100 nM HcA or HcHA in high
641 K⁺ buffer, which contains (mM): NaCl 140, KCl 3, KH₂PO₄ 1.5, Na₂HPO₄ 8, MgCl₂ 0.5, and
642 CaCl₂ 1, for 5 minutes at 37°C. Cells were then washed three times with phosphate-buffered
643 saline (PBS). Binding of HcA or HcHA was examined using two complementary approaches. (1)
644 Immunostaining: neurons were fixed with 4% paraformaldehyde and permeabilized with 0.3%
645 Triton X-100 in PBS solution. Images were collected using a Leica TCS SP8 confocal
646 microscope with a 40X oil objective. (2) Immunoblot analysis: neurons were harvested in a lysis
647 buffer (PBS with 1% Triton X-100, 0.05% SDS and protease inhibitor cocktail (Roche, CA), 100
648 μ l per one well of 24-well plates). Lysates were centrifuged for 10 minutes at 4°C and the
649 supernatants were subjected to SDS-PAGE and western blot analysis. Binding of HcA or HcHA
650 were detected using a monoclonal human anti-HcA antibody (RAZ-1), which recognizes both
651 HcA and HcHA. It also recognizes mutants of HcA and HcHA examined in this study with
652 similar sensitivity (“input” lanes in Figs. 4b and 6b)

653 **Entry of BoNTs into neurons.** Neurons were exposed to 1 nM BoNT/A1 and 0.1 nM BoNT/D
654 in high K⁺ buffer for 5 minutes at 37°C. Cells were washed three times with PBS and further

655 incubated in toxin-free media for 8 hrs. Neuron lysates were then harvested and subjected to
656 immunoblot analysis, detecting cleavage of toxin substrate SNAP-25 (for BoNT/A1) and
657 VAMP2 (for BoNT/D). Cleavage of SNAP-25 by BoNT/A1 generates a smaller fragment that
658 can be detected on immunoblot. Cleavage of VAMP2 by BoNT/D resulted in a loss of
659 immunoblot signal of VAMP2.

660 **Mouse phrenic nerve hemidiaphragm (MPN) assay.** The MPN assay was performed as
661 described previously employing 20-30 g NMRI mice (Janvier SA, France)^{20,21}. The phrenic
662 nerve was continuously stimulated at 5-25 mA with a frequency of 1 Hz and with a 0.1 ms pulse
663 duration. Isometric contractions were transformed using a force transducer and recorded with
664 VitroDat Online software (FMI GmbH, Germany). The time required to decrease the amplitude
665 to 50% of the starting value (paralytic half-time) was determined. To allow comparison of the
666 altered neurotoxicity of mutants with H6tBoNTA wild-type, a power function ($y(\text{H6tBoNTA};$
667 $10, 30, 80 \text{ pM}) = 139.6x^{-0.1957}$, $R^2 = 0.9991$) was fitted to a concentration-response-curve
668 consisting of three concentrations determined minimum in technical triplicates. Resulting
669 paralytic half-times of the H6tBoNTA mutants were converted to concentrations of the wild-type
670 employing the above power functions and finally expressed as relative neurotoxicity.

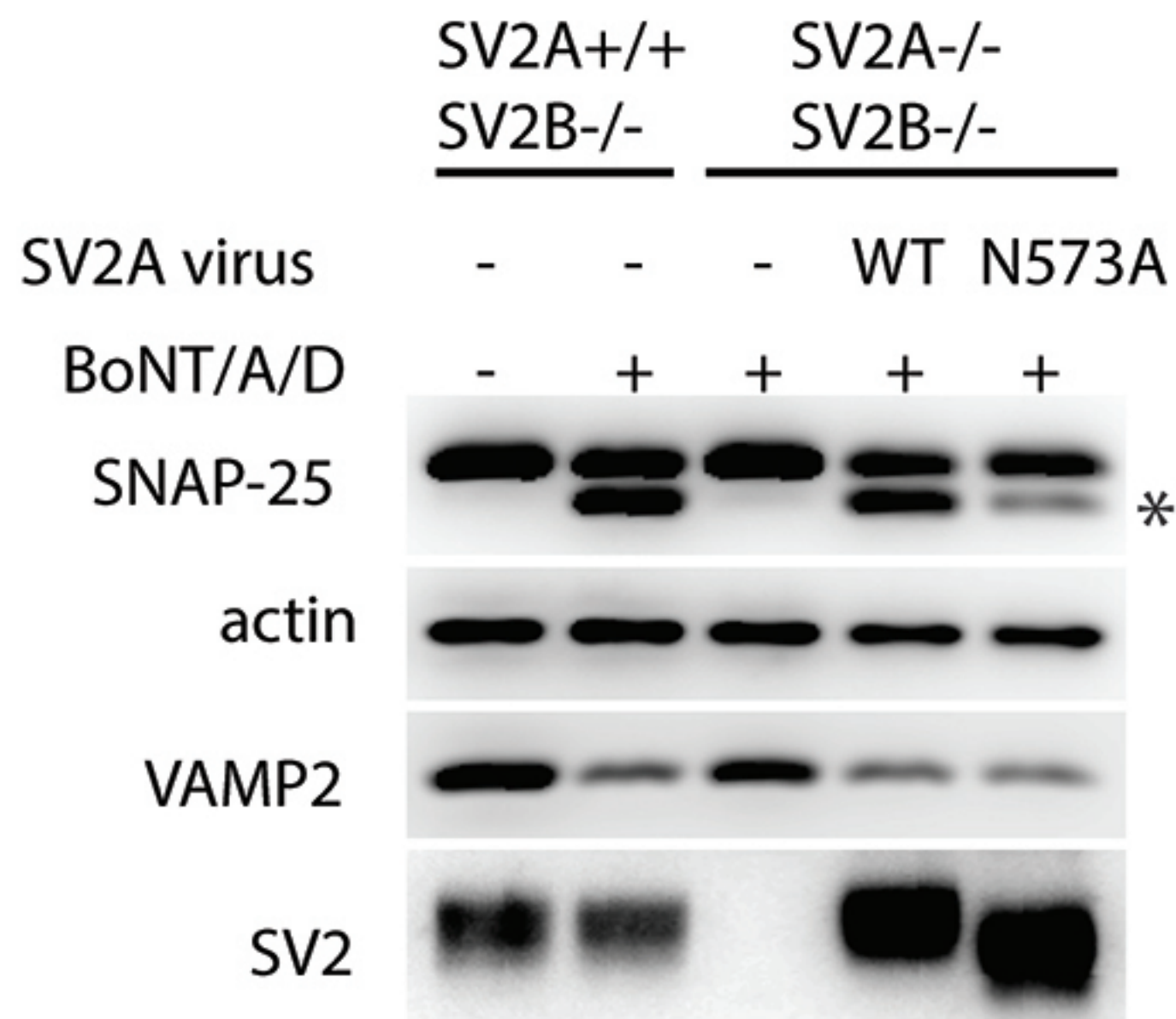
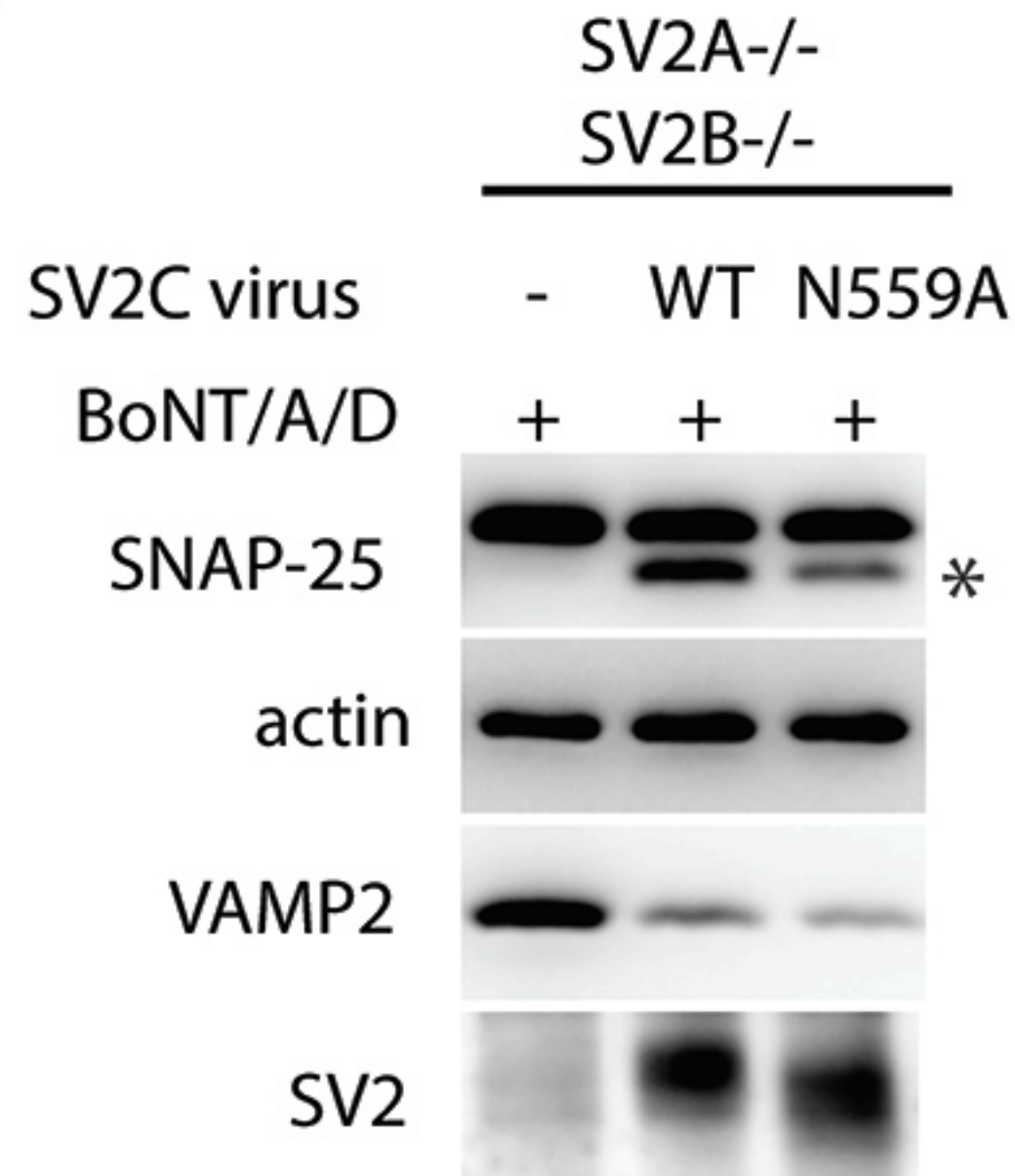
671

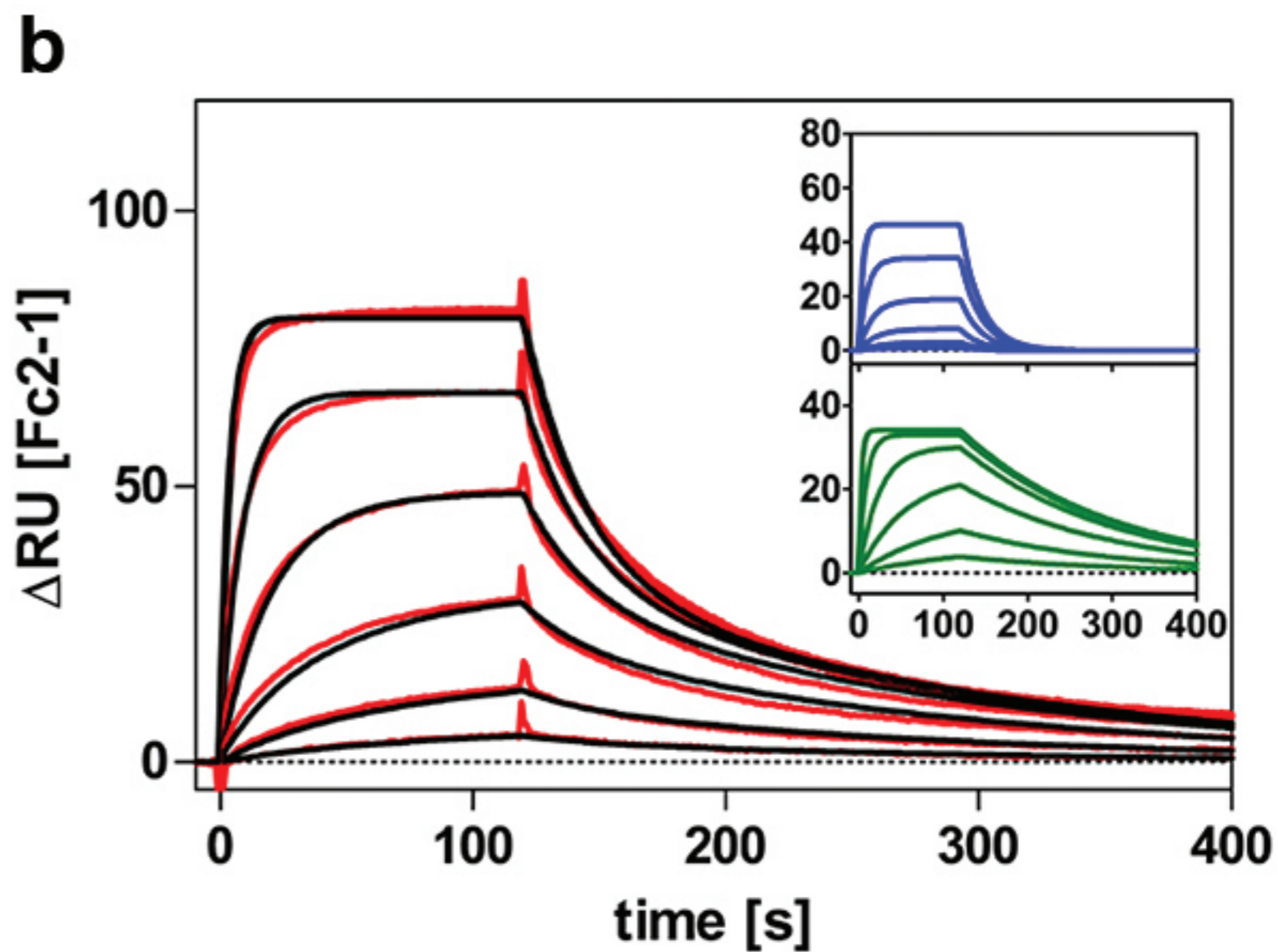
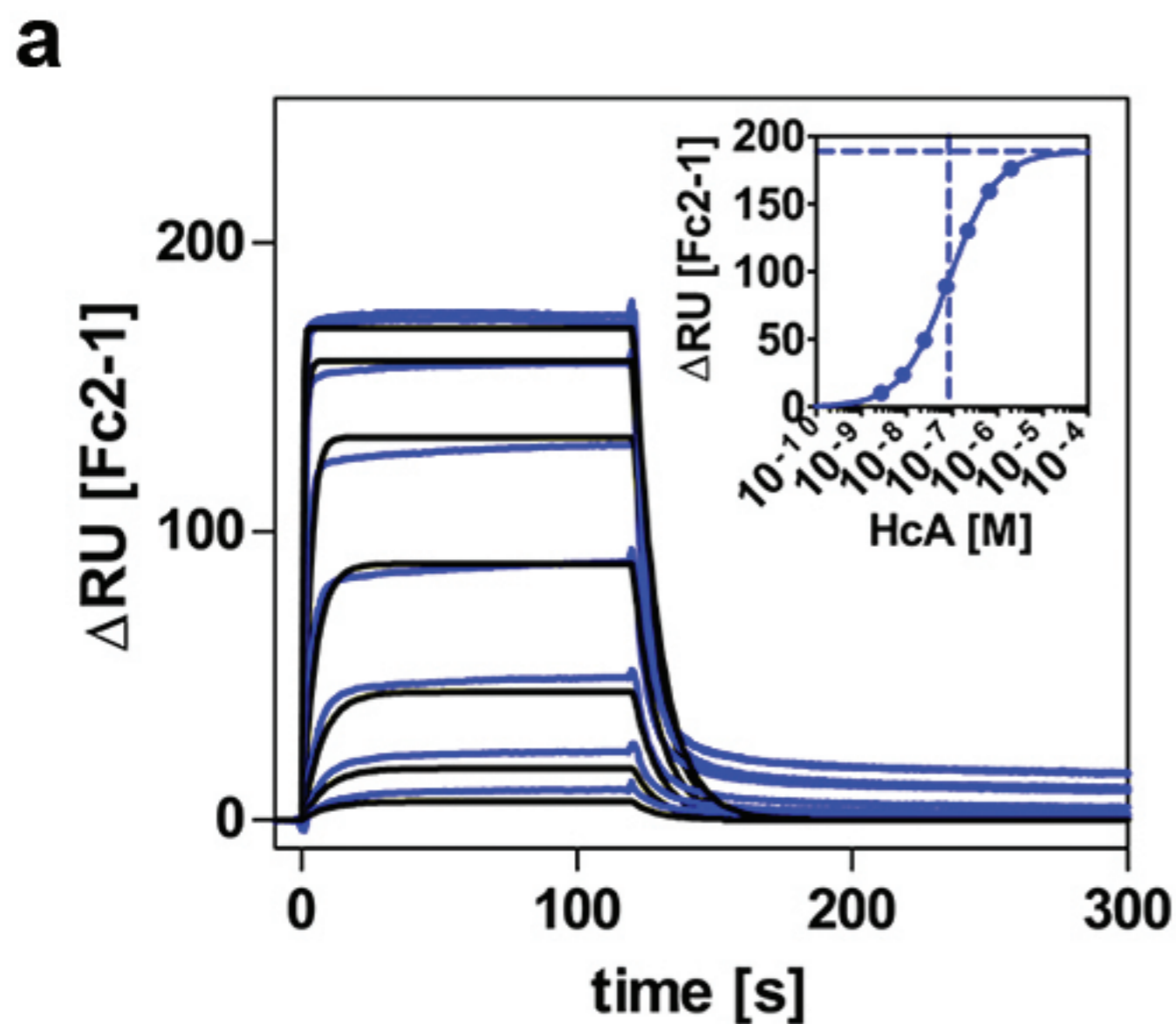
672 REFERENCES

673

- 674 39. Kabsch, W. Xds. *Acta Crystallogr D Biol Crystallogr* **66**, 125-32 (2010).
- 675 40. McCoy, A.J. et al. Phaser crystallographic software. *J Appl Cryst* **40**, 658-74 (2007).
- 676 41. Emsley, P. & Cowtan, K. Coot: model-building tools for molecular graphics. *Acta*
677 *Crystallogr D Biol Crystallogr* **60**, 2126-32 (2004).
- 678 42. Potterton, E., Briggs, P., Turkenburg, M. & Dodson, E. A graphical user interface to the
679 CCP4 program suite. *Acta Crystallogr D Biol Crystallogr* **59**, 1131-7 (2003).
- 680 43. Brunger, A.T. Free R value: a novel statistical quantity for assessing the accuracy of
681 crystal structures. *Nature* **355**, 472-5 (1992).
- 682 44. Chen, V.B. et al. MolProbity: all-atom structure validation for macromolecular
683 crystallography. *Acta Crystallogr D Biol Crystallogr* **66**, 12-21 (2010).
- 684 45. Myszka, D.G. Improving biosensor analysis. *J Mol Recognit* **12**, 279-84 (1999).

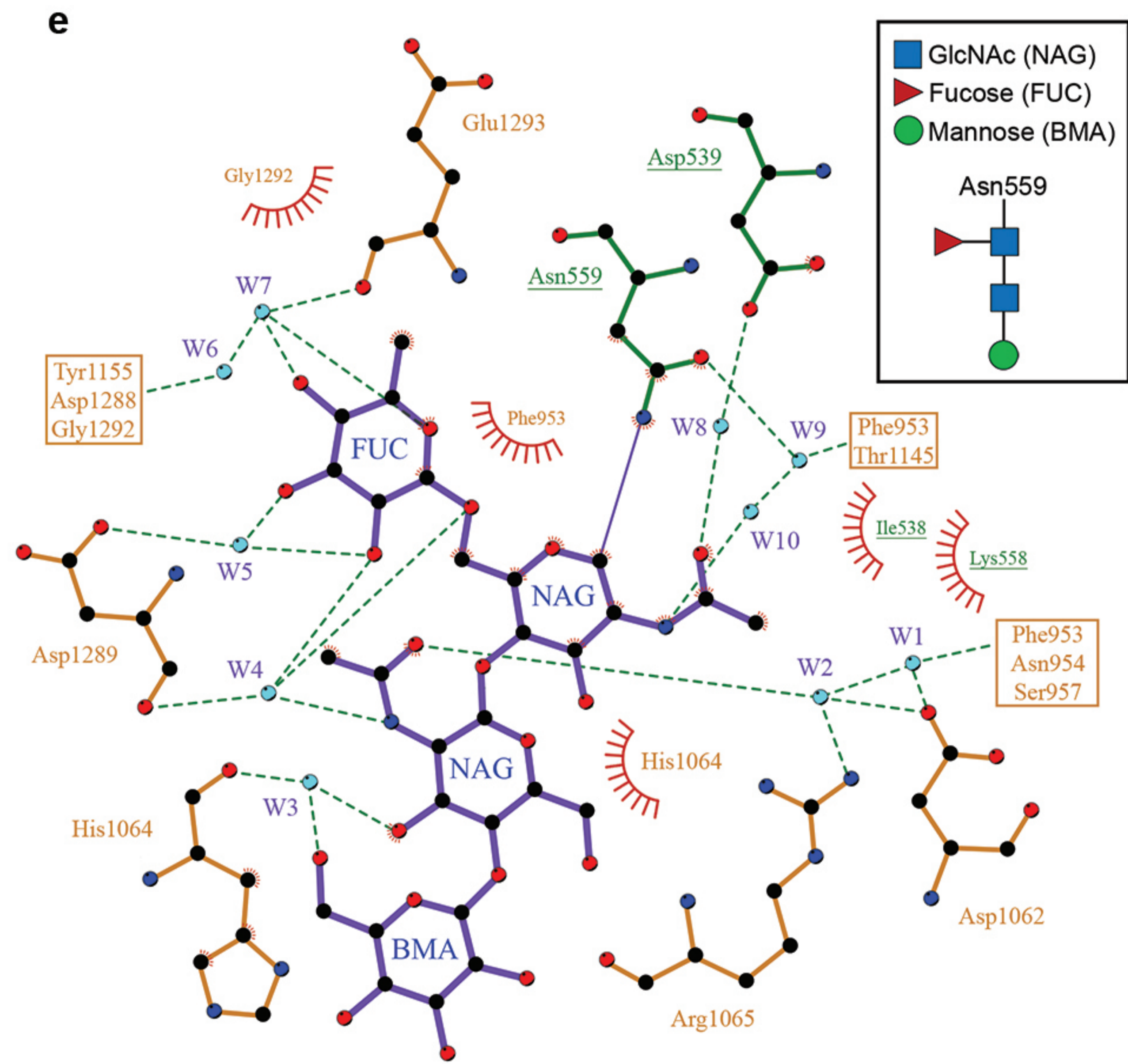
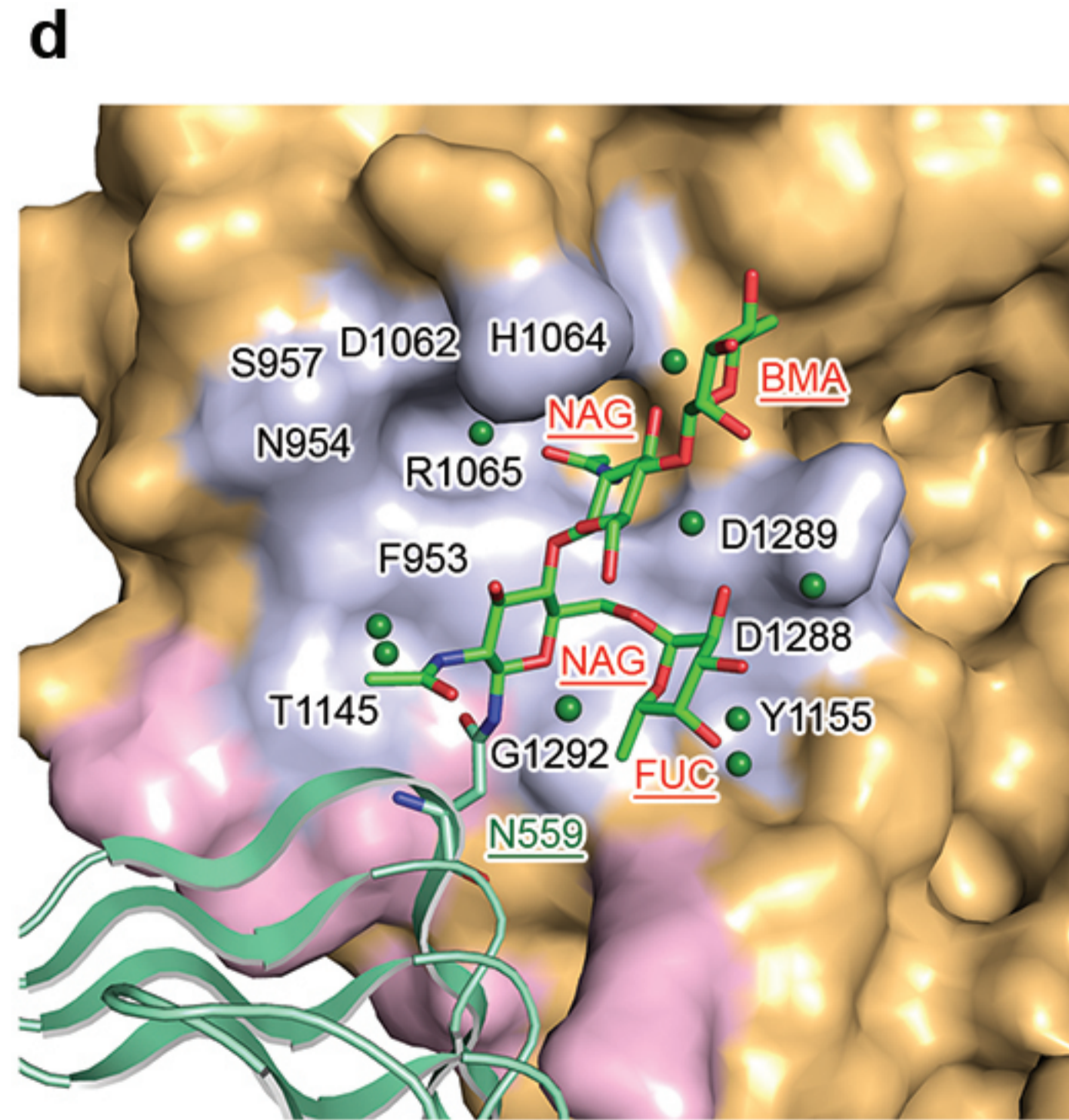
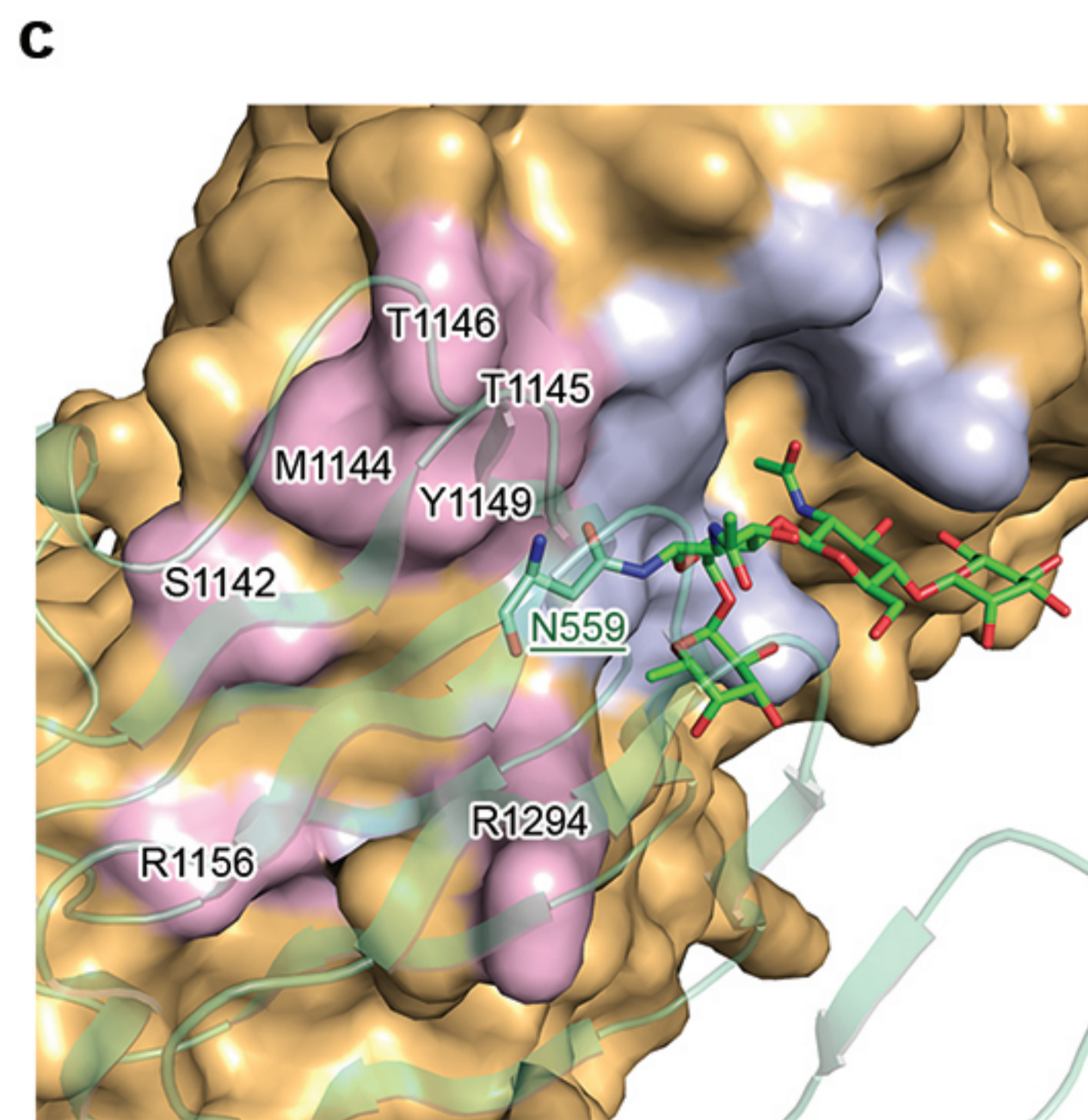
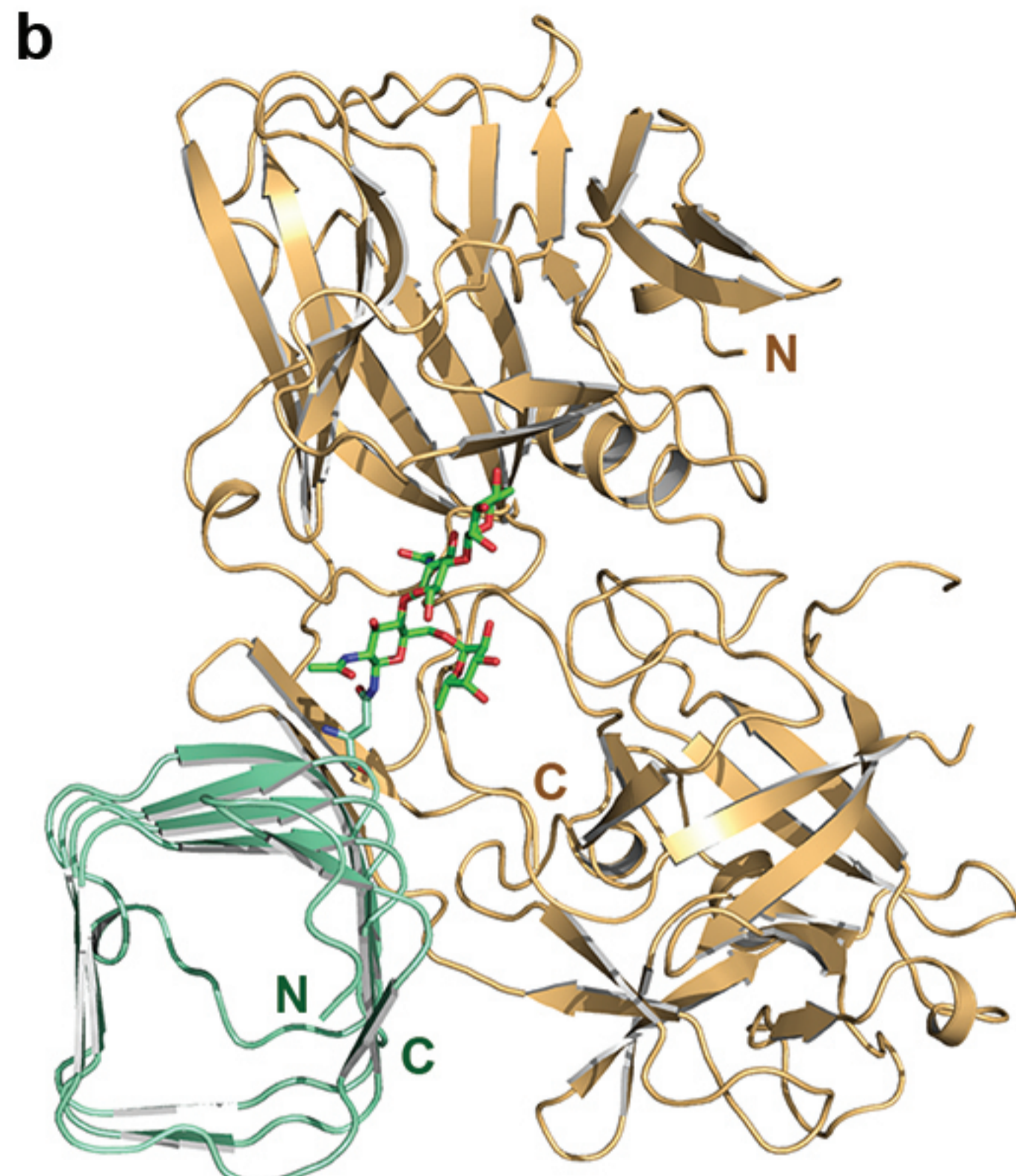
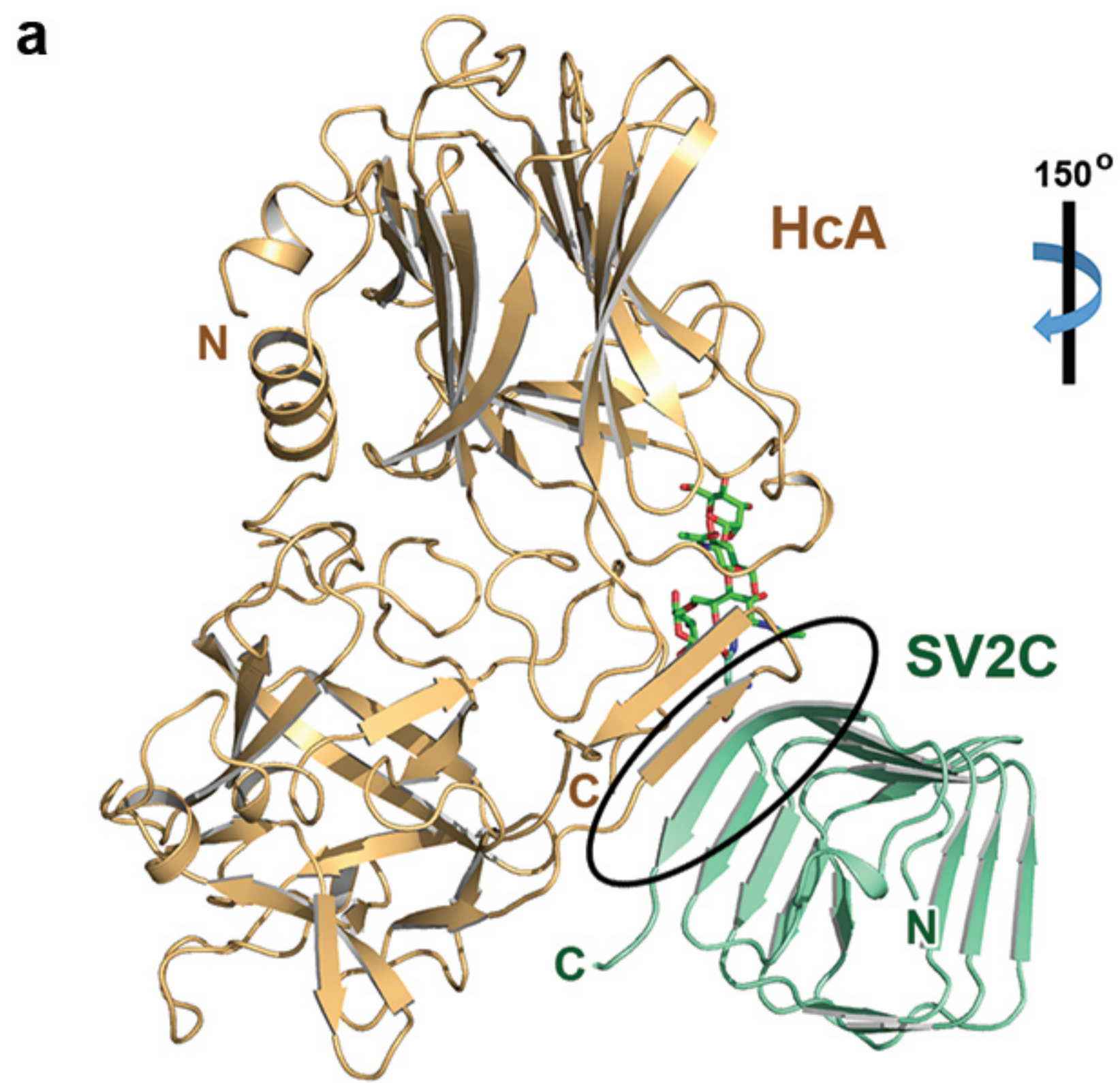
685

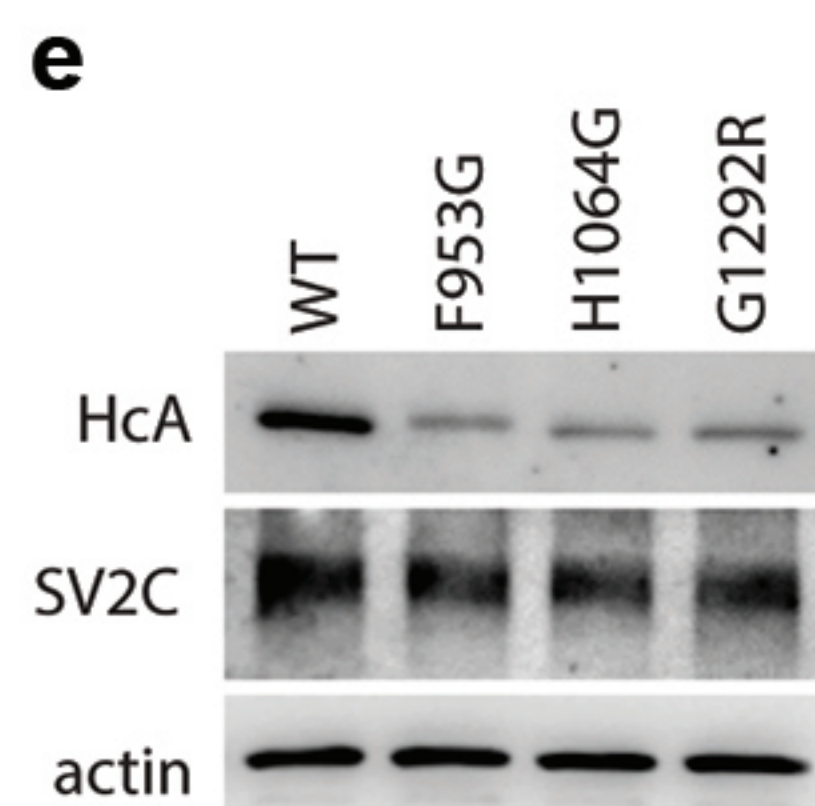
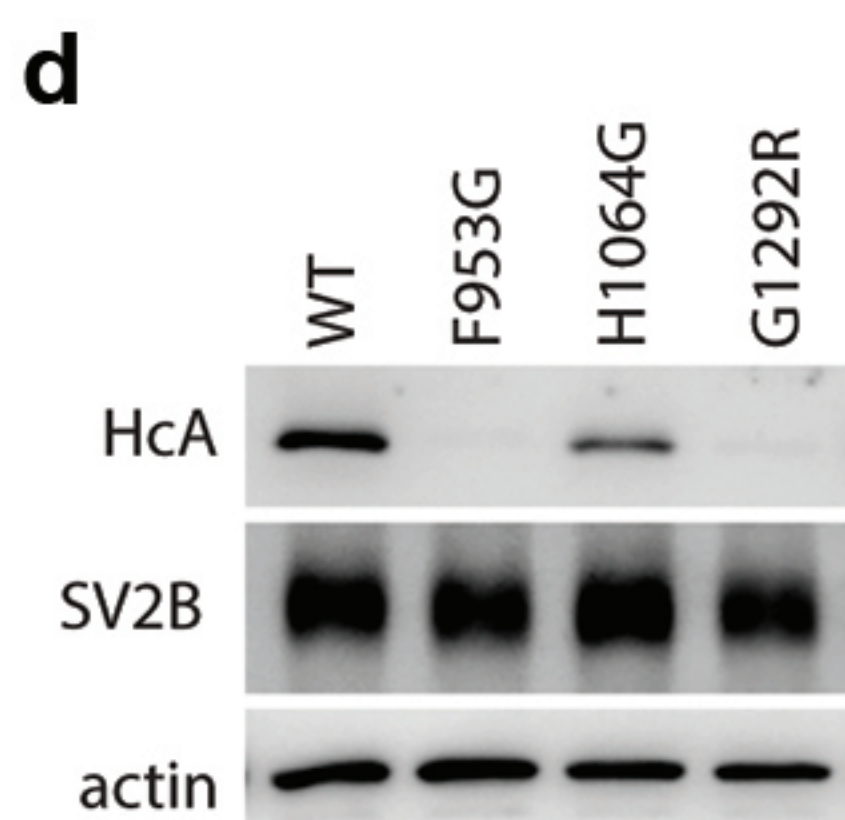
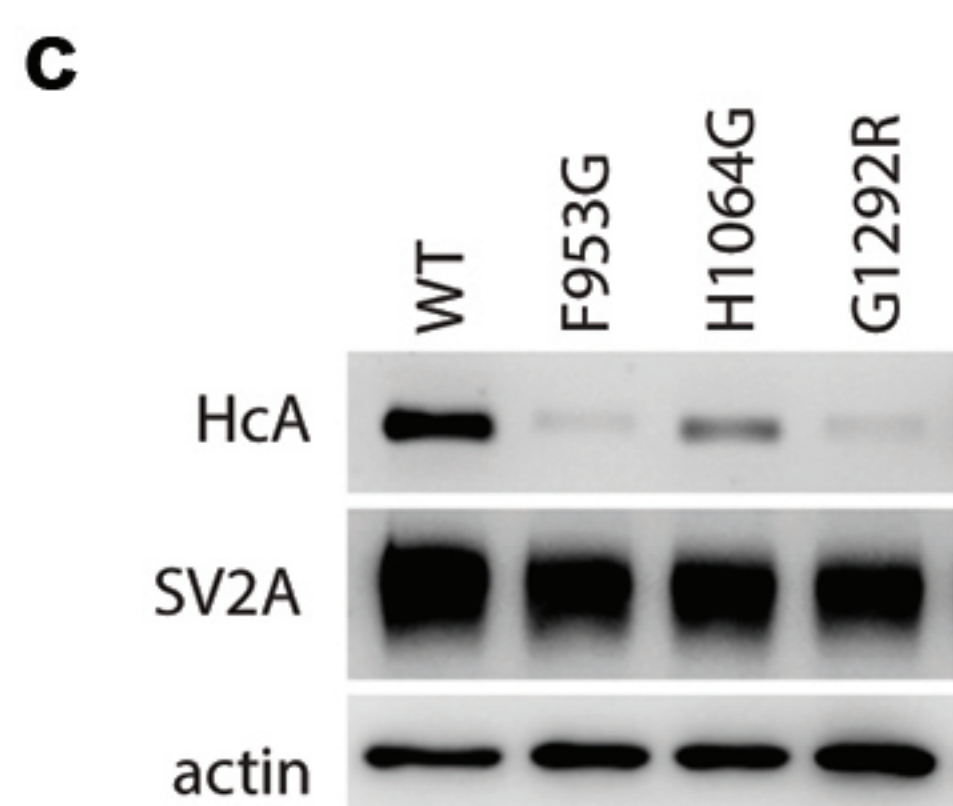
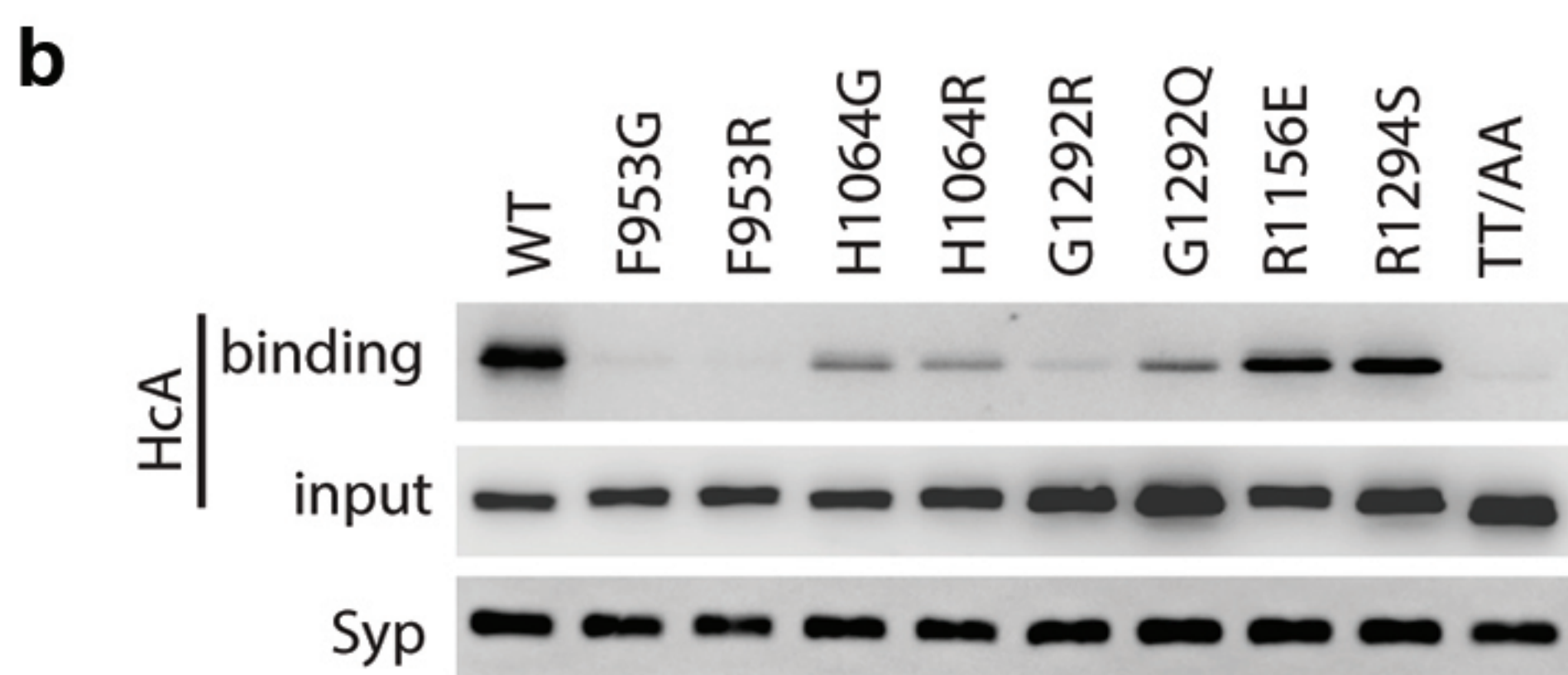
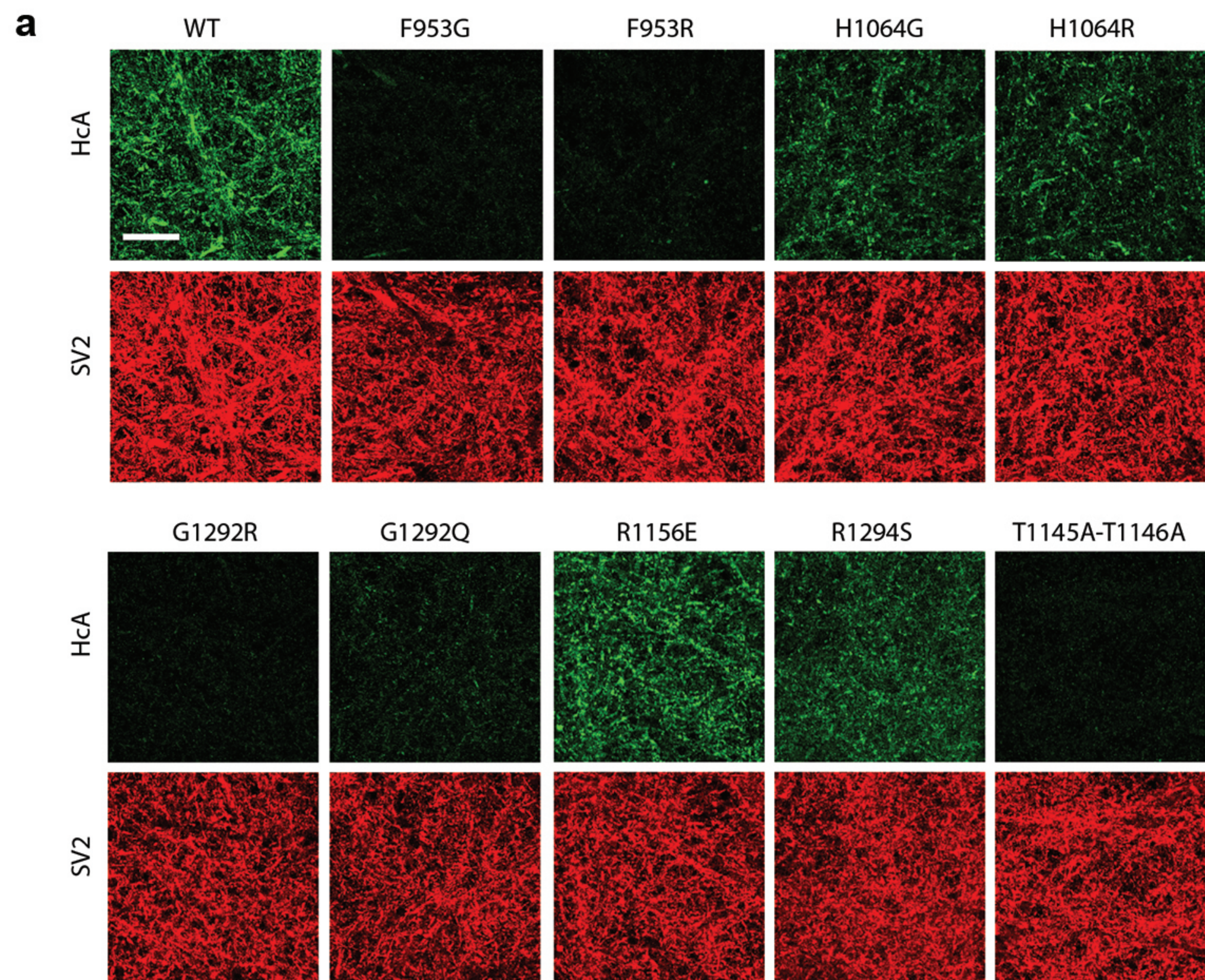
a**b**

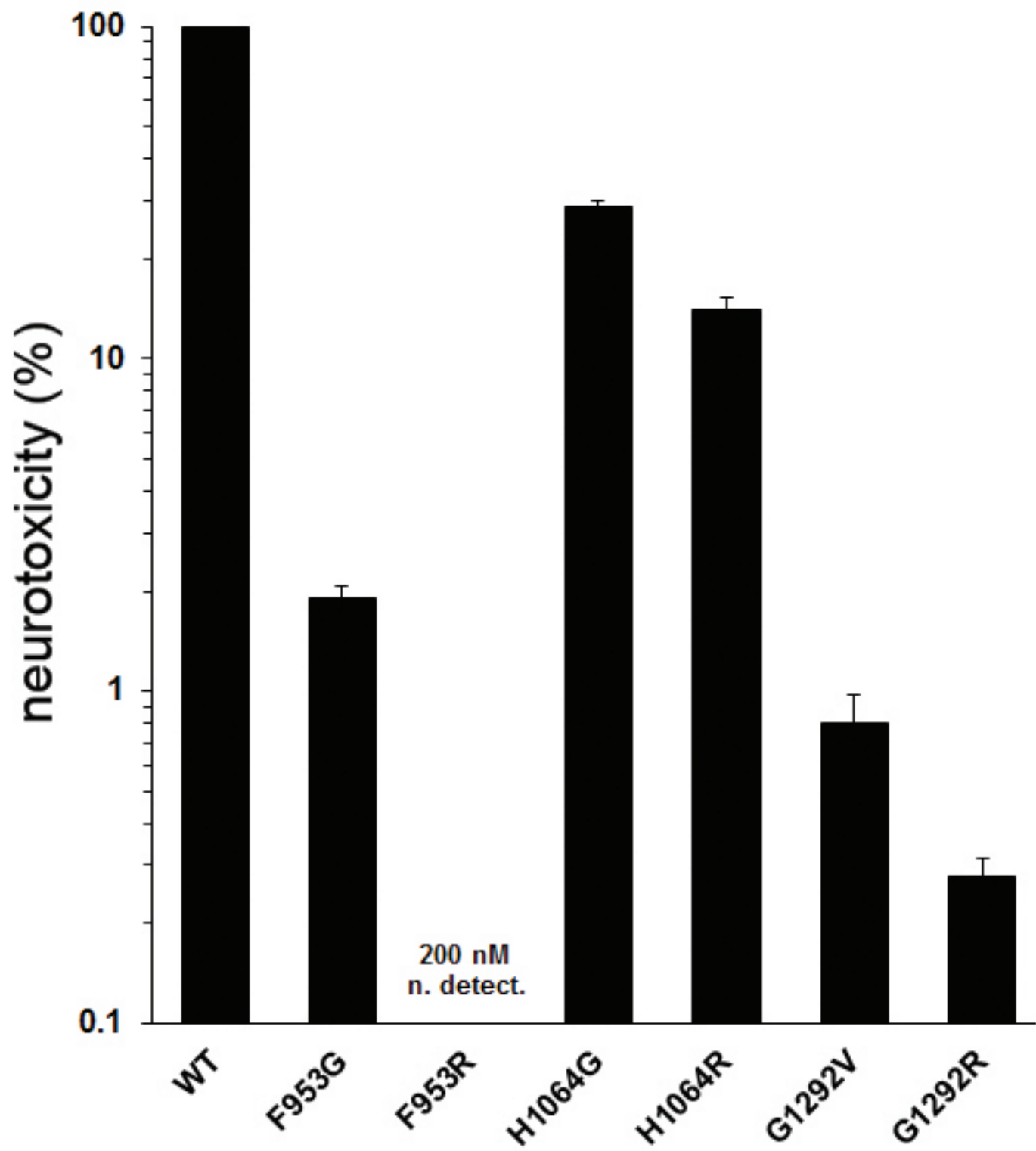


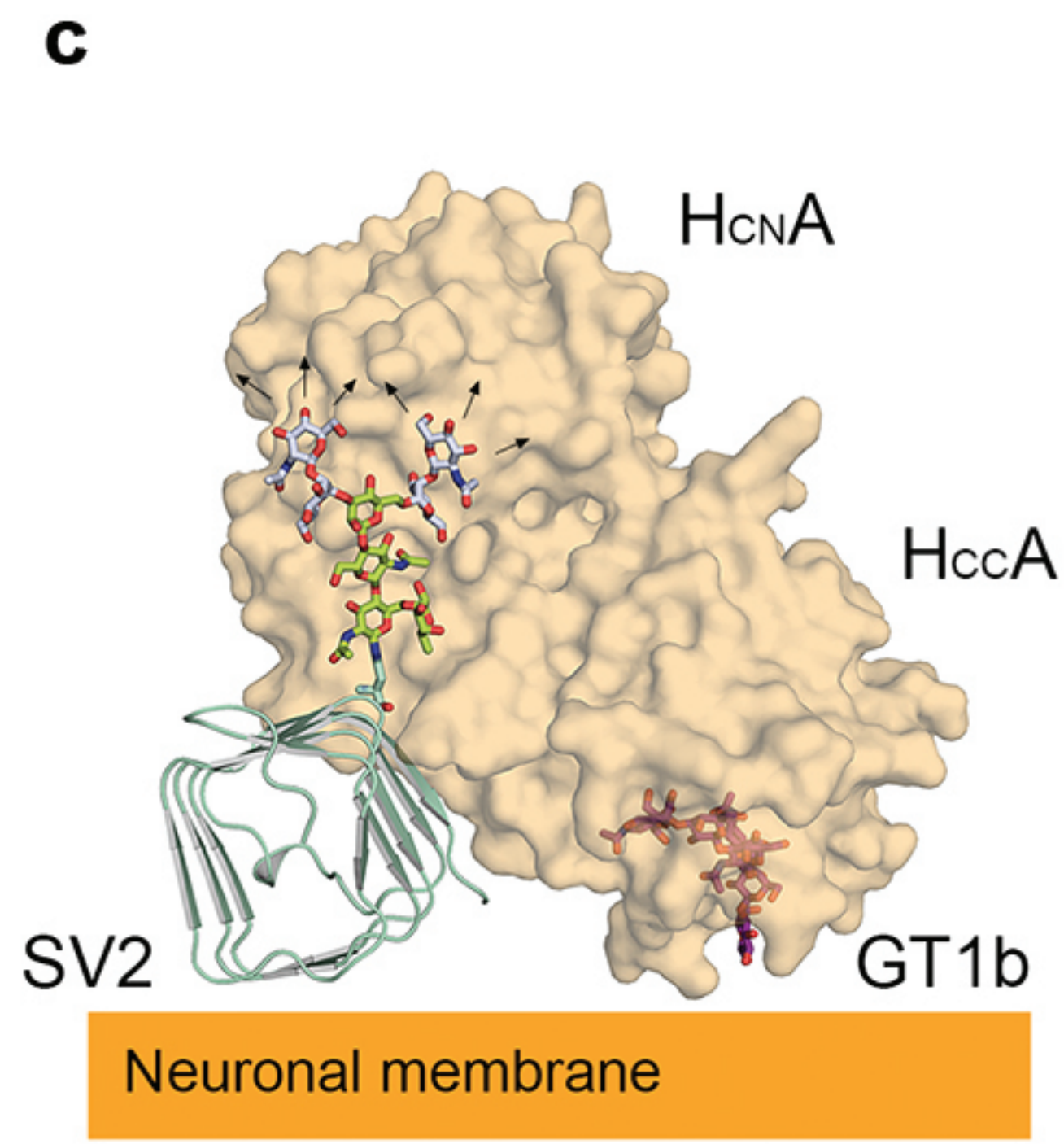
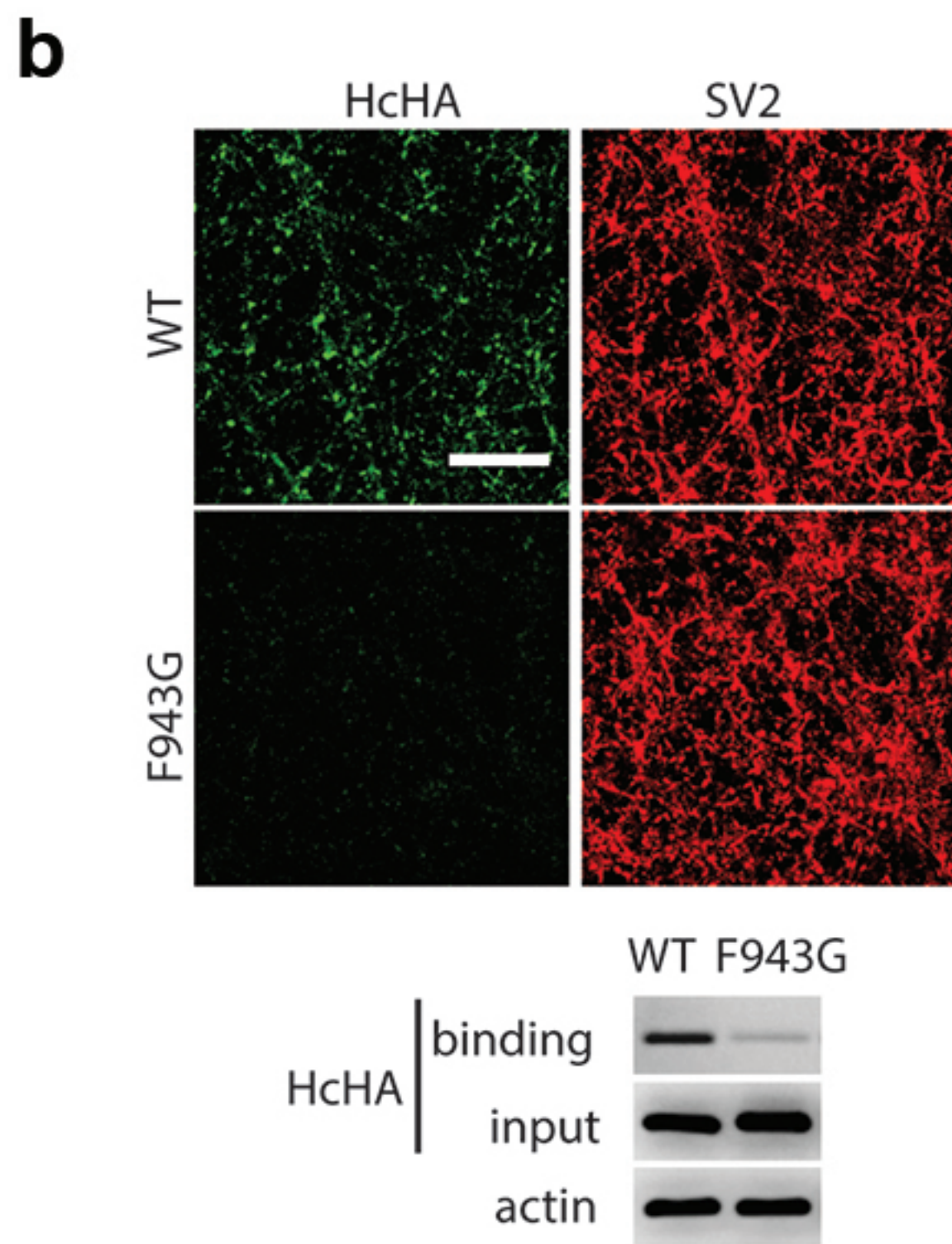
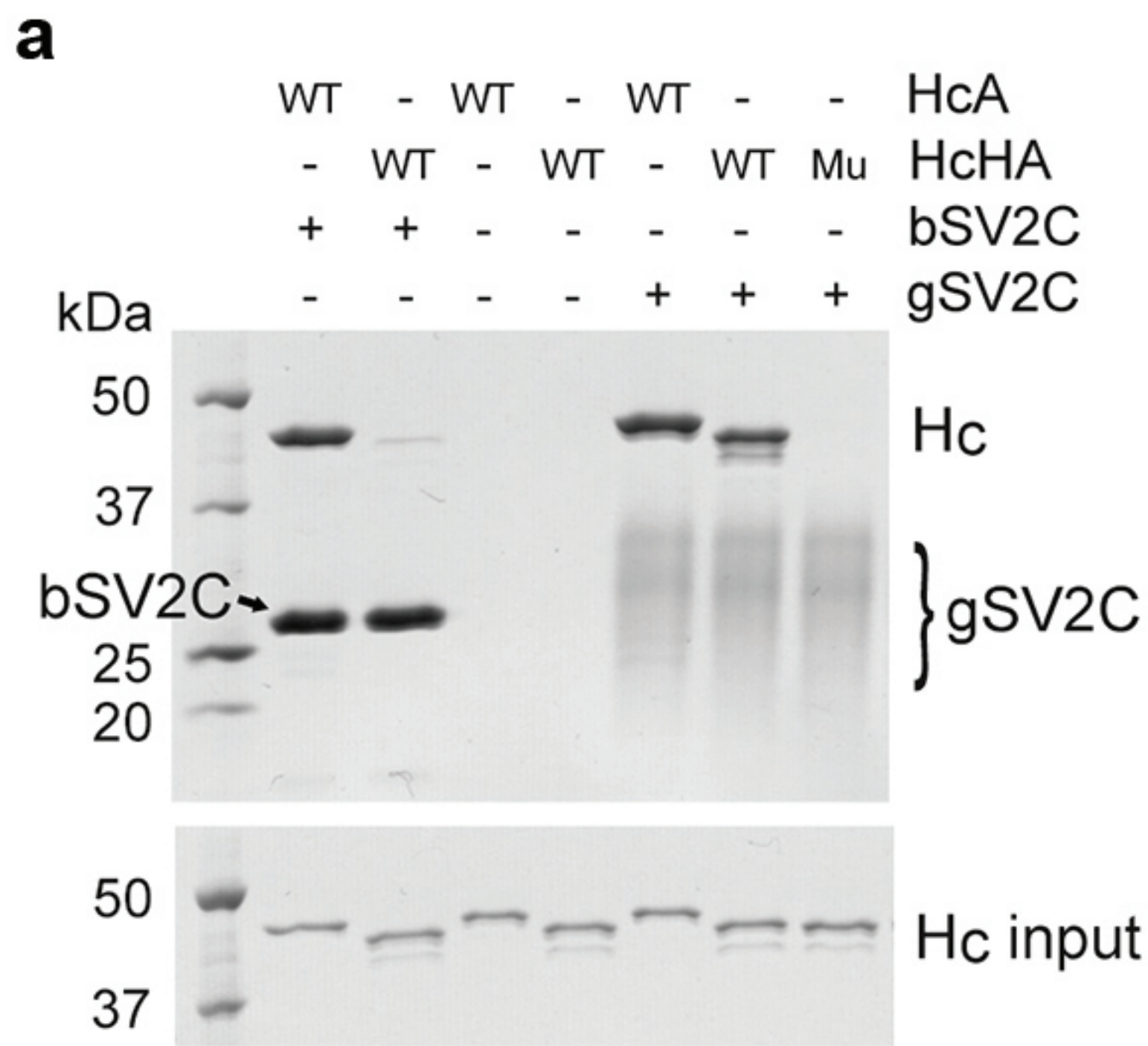
c

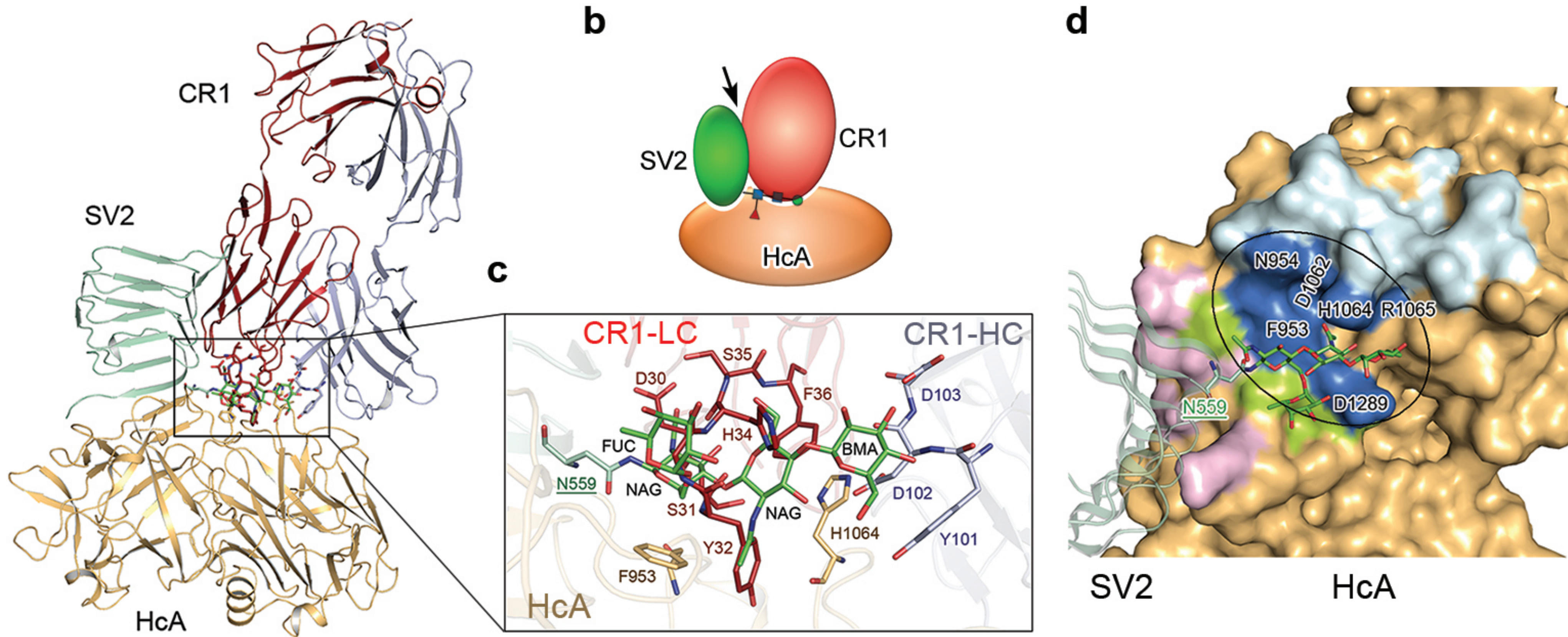
	k_a [$M^{-1}s^{-1}$]	k_d [s^{-1}]	K_D kinetics [M]	K_D steady state [M]
bSV2C	$1.5 \pm 0.0 \times 10^6$	$1.1 \pm 0.0 \times 10^{-1}$	$7.2 \pm 0.2 \times 10^{-8}$	$8.6 \pm 0.6 \times 10^{-8}$
gSV2C	$1.7 \pm 0.0 \times 10^5$	$3.7 \pm 0.0 \times 10^{-2}$	$2.2 \pm 0.0 \times 10^{-7}$	n.a.
	$3.4 \pm 0.1 \times 10^5$	$4.9 \pm 0.4 \times 10^{-3}$	$1.5 \pm 0.2 \times 10^{-8}$	

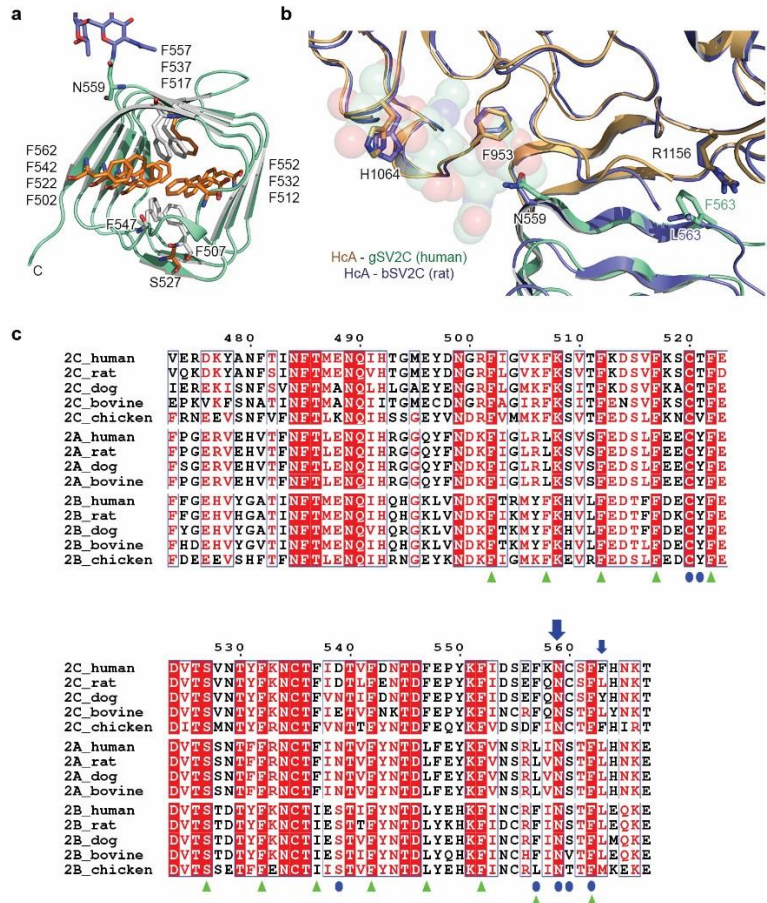








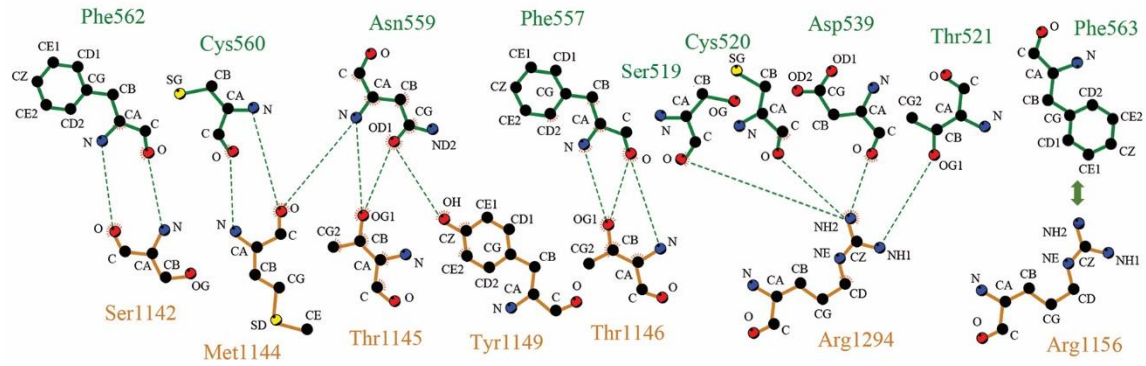




Supplementary Figure 1

SV2 has a unique structure.

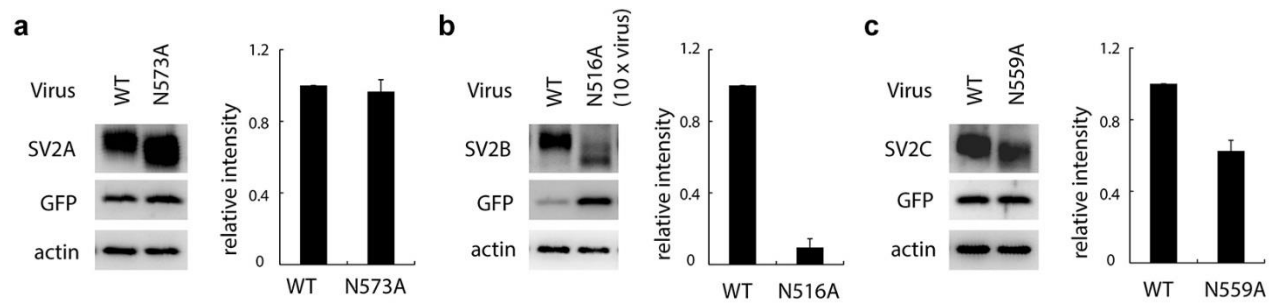
(a) The structure of human gSV2C displays a unique pentapeptide-repeat motif, where phenylalanine residues, except S527, spaced 5 residues apart provide important stacking effect to stabilize the structure. These residues are shown in sticks, with the ones that are conserved in all three SV2 isoforms across different species are colored gold. (b) The structures of H_cA in complex with the rat bSV2C or human gSV2C are superimposed. The N559 glycan of gSV2C is shown as a transparent sphere model. Residue F563 of human SV2C is replaced by L563 in rat SV2C, which abolishes the cation- π stacking interaction. (c) Representative sequences of SV2A, SV2B, and SV2C were selected from different species: human SV2A (NP_055664.3), 2B (CAG33367.1), 2C (AAI00828.1); rat SV2A (NP_476558.2), 2B (NP_476555.1), 2C (NP_113781.1); dog SV2A (XP_003639668.1), 2B (XP_005618386.1), 2C (XP_546060.2); bovine SV2A (NP_776387.1), 2B (NP_001076917.1), 2C (NP_001178948.1); chicken SV2B (XP_425081.2), 2C (XP_429151.3). Sequence alignments were made using Clustal Omega¹ and ESPrpt². Only the truncated loop 4 of SV2 is shown for clarity. Identical residues are indicated with white letters on a red background, similar conserved residues are in red letters, varied residues are in black letters. The residues of SV2C that directly bind to H_cA are indicated by blue ovals; the pentapeptide-repeat is labeled by green triangles. The N-linked glycosylation site, N559, is highly conserved, but not F563 (blue arrows).



Supplementary Figure 2

The protein-protein interactions between H_cA and the human gSV2C.

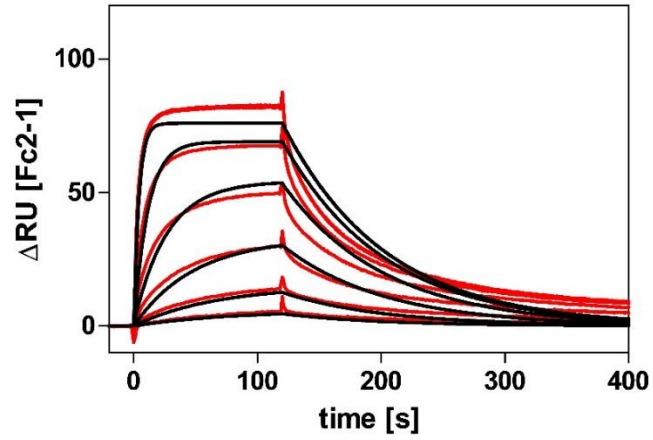
The plots were generated using LIGPLOT³. BoNT/A and SV2C residues are labeled brown and green, respectively. Hydrogen bonds are indicated by dashed green lines. A similar interaction network is observed in the structure of H_cA in complex with the rat bSV2C, except that the cation- π stacking interaction (double arrow) is unique for human SV2C.



Supplementary Figure 3

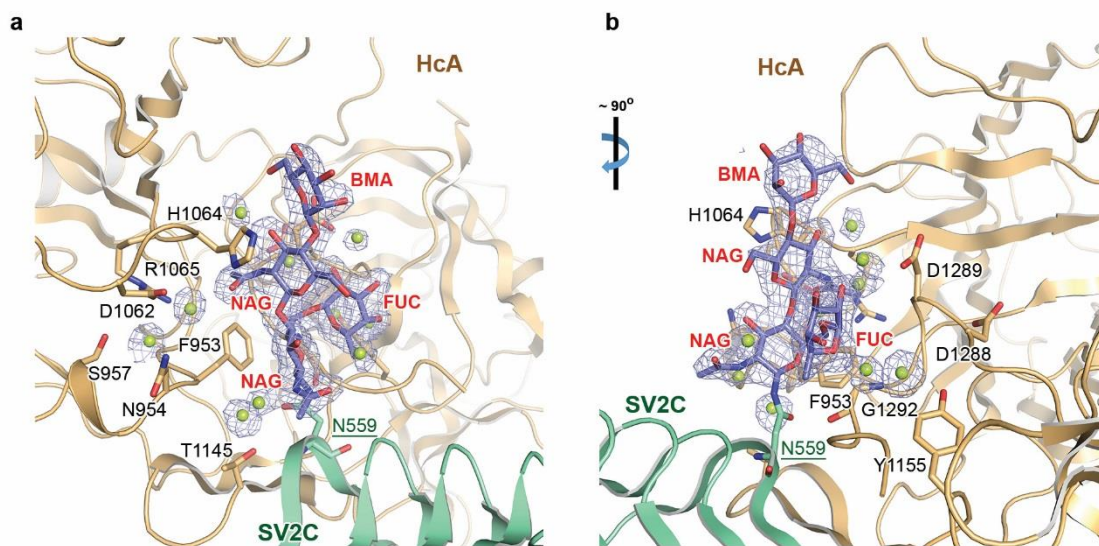
Expression levels of the deglycosylation mutants of SV2A, 2B, and 2C in neurons.

Hippocampal/cortical neurons cultured from SV2A(-/-)SV2B(-/-) mice were infected with lentiviruses that express either WT SV2A, 2B, and 2C, or indicated deglycosylation mutants. Cell lysates were harvested and subjected to immunoblot analysis. Actin served as a loading control. The lentiviral vector contains two separated synapsin promoters, with one driving expression of SV2 and the other driving expression of GFP. Thus, GFP served as an internal control for viral infection. Immunoblot signals of SV2 were quantified, normalized using GFP signals, and compared between WT and deglycosylation mutants. The same amounts of viruses were used for WT SV2A and SV2A-N573A (panel **a**), and for WT SV2C and SV2C-N559A (panel **c**). The deglycosylation mutation has no effect on SV2A and modestly reduced the expression level of SV2C in neurons. However, it severely reduced the expression level of SV2B. As shown in panel **b**, even with 10-fold more viruses, SV2B-N516A expression was still drastically lower than WT SV2B. The data are presented as mean \pm S.D., n = 3.



Supplementary Figure 4

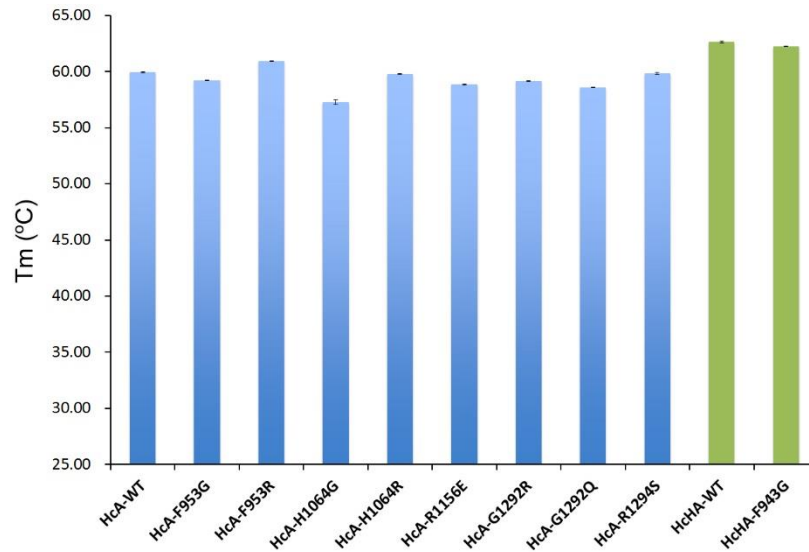
SPR binding curves of H_cA and gSV2C (red) overlaid with a 1:1 Langmuir binding model fit (black). Clear deviations were observed between the measured sensorgrams and the fit.



Supplementary Figure 5

Electron densities of the N559 glycan of SV2C in the gSV2C-H_cA complex.

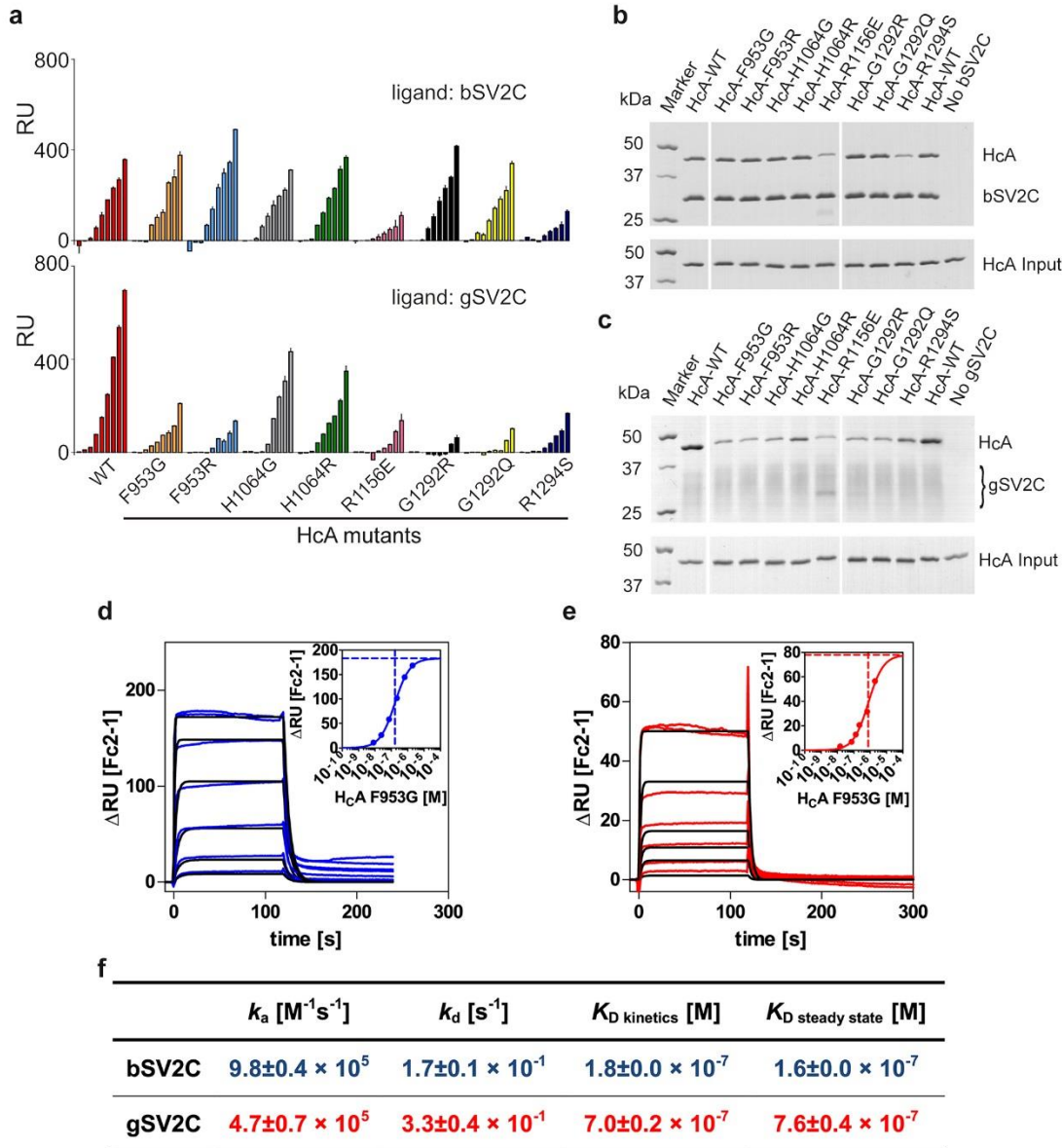
(a) Key glycan-binding residues of H_cA and the N559 glycan are shown as stick models. Water molecules facilitating the H_cA-glycan association are shown as green spheres. A simulated-annealing omit electron density map contoured at 1.5 σ was overlaid with the final refined model. (b) A different view with a rotation $\sim 90^\circ$ about a vertical axis.



Supplementary Figure 6

Single-site mutations of HcA and HcHA adopt wild-type-like structures.

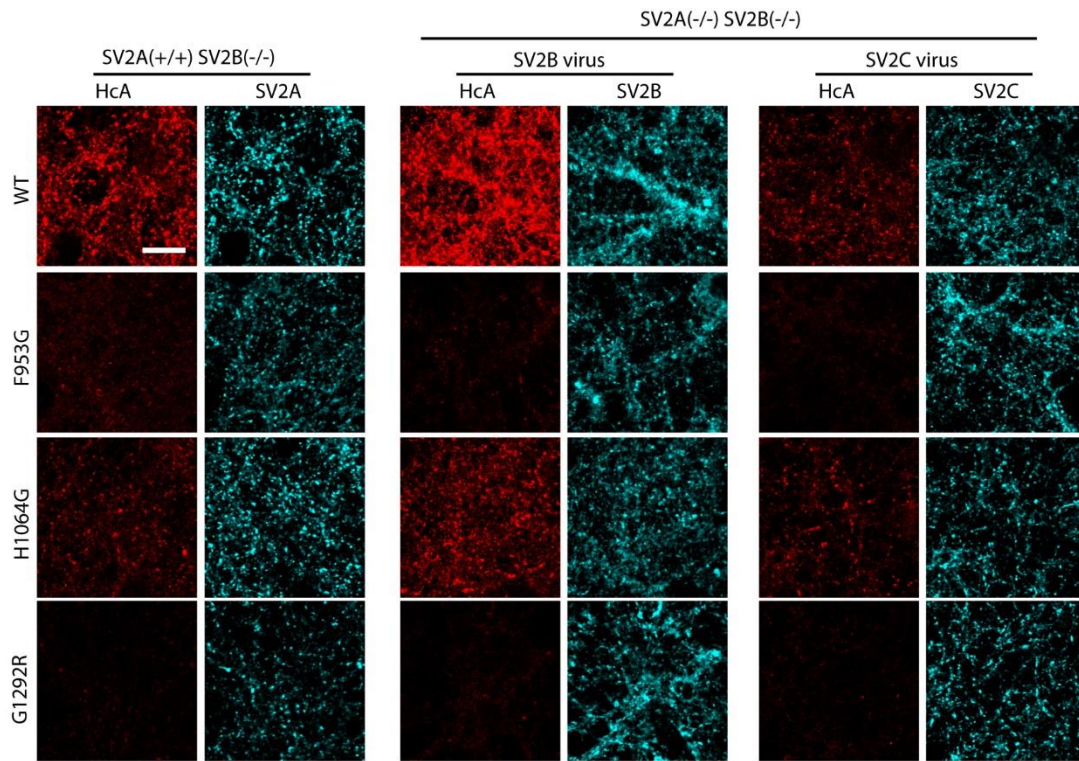
The thermal stability of proteins was measured using a fluorescence-based thermal shift assay on a StepOne real-time PCR system (ThermoFisher)⁴. Specifically, protein melting was monitored using a hydrophobic dye, SYPRO Orange (Sigma-Aldrich), as the temperature was increased in a linear ramp from 20°C to 95°C. The midpoint of the protein-melting curve (T_m) was determined using the software provided by the instrument manufacturer. The data are presented as mean ± S.D., n = 3. All HcA and HcHA mutants showed T_m values comparable to the wild-type protein, indicating correct protein folding.



Supplementary Figure 7

Characterization of bindings between HcA variants and human bSV2C and gSV2C, respectively.

(a) Surface plasmon resonance was used to examine the changes of binding affinity between HcA variants and SUMO-bSV2C or gSV2C, respectively. SV2C was covalently immobilized to a CM5 chip as a ligand whereas HcA variants were analytes. Bars from left to right represent the responses when HcA was applied at 10 pM, 1 nM, 10 nM, 25 nM, 50 nM, 75 nM, 100 nM, and 200 nM, respectively. RU stands for arbitrary response unit. (b-c) Interactions between HcA variants (preys) and SUMO-bSV2C or gSV2C (baits) were examined by a pull down assay. (d-f) Binding kinetics and affinity between HcA-F953G and immobilized bSV2C (107 RU; panel d) or gSV2C (74 RU; panel e) were determined by injecting 1:3 dilution series ranging from 2,000 nM to 8.23 nM. Values shown represent the mean \pm S.D. (n = 2).



Supplementary Figure 8

Binding of glycan-binding deficient H_CA mutants to neurons that express individual SV2 isoforms.

Hippocampal/cortical neurons cultured from SV2A(+/+)SV2B(-/-) mice served as neurons that only express SV2A. Neurons that only express SV2B or SV2C were created by infecting neurons cultured from SV2A(-/-)SV2B(-/-) mice with lentiviruses that express SV2B or SV2C, respectively. Neurons were then exposed to WT or indicated H_CA mutant (100 nM, 5 min), washed, fixed, and subjected to immunostaining analysis. H_CA was detected with a monoclonal human anti-BoNT/A antibody (RAZ-1) and SV2 was detected with a mouse monoclonal pan-SV2 antibody. Scale bar, 20 μm.

880 890 900 910 920

BoNT/A1 NIINTSILNLRYES.NHLIDLSRYASKINIGSRVNFDPIDKNOIQOLFPLESSKIEVILK
 BoNT/A2 NIVNTSILSIVYKK.DDLIDLSRYGAKINIGDRVYYSIDKNOIKLPLESSKIEVILK
 BoNT/A3 NIVNTSILSIVYKK.DDLIDLSRYGAKINIGDRVYYSIDKNOIKLPLESSKIEVILK
 BoNT/A4 NITNASILSIVYKD.DDLIDLSRYGAEIYNGDKVYNSIDKNOIKLPLESSKIEVILK
 BoNT/A5 NIINTSILNLRYES.NHLIDLSRYASEINIGSRVNFDPIDKNOIQOLFPLESSKIEVILK
 BoNT/A6 NIINTSILSLRYEN.NHLIDLSRYASKINIGSRVNFDPIDKNOIQOLFPLESSKIEVILK
 BoNT/A7 NIINTSILNLRYES.NHLIDLSRYASKINIGSRVNFDPIDKNOIQOLFPLESSKIEVILK
 BoNT/A8 NITNTSILSIVVDK.DGRIDLSRYGAEIYNGDKVSYNSIDKNOIKLPLESSKIEVILK
 BoNT/HA ELKYNCILNLIKYEEMDRDKLVDSSGYRSRINIGTGVKFSIDKNOIQOLFPLESSKIEVILK

930 940 950 960 970 980

BoNT/A1 NAIVNSMYENFSTSFWRIPKYFNSISLNNEYTINCIMENNSGWKVSINYG...EIIW
 BoNT/A2 NAIVNSMYENFSTSFWRIPKYFSKINLNNEYTINCIEENNSGWKVSINYG...EIIW
 BoNT/A3 NAIVNSMYENFSTSFWRIPKYFSKINLNNEYTINCIEENNSGWKVSINYG...EIIW
 BoNT/A4 KAIVNSMYENFSTSFWRIPKYFNSISLNNEYTINCIMENNSGWKVSINYG...EIIW
 BoNT/A5 NAIVNSMYENFSTSFWRIPKYFSKINLNNEYTINCIEENNSGWKVSINYG...EIIW
 BoNT/A6 NAIVNSMYENFSTSFWRIPKYFSKINLNNEYTINCIEENNSGWKVSINYG...EIIW
 BoNT/A7 NAIVNSMYENFSTSFWRIPKYFSKINLNNEYTINCIEENNSGWKVSINYG...EIIW
 BoNT/A8 NAIVNSMYENFSTSFWRIPKYFSKINLNNEYTINCIEENNSGWKVSINYG...EIIW
 BoNT/HA NGVIYNSMYENFSTSFWRIPKYFRN...INNEYKITSMONGWKEVSLNFSNMNSKIIW

990 1000 1010 1020 1030 1040

BoNT/A1 TLDQTQEIQRVVFKYSQMINISDYINRWIEVITNNRRLNNSKIYINGRLIDQKPIISNLG
 BoNT/A2 TLDQNKQNIQRVVFKYSQMVNISDYINRWIEVITNNRRLTKSKYIINGRLIDQKPIISNLG
 BoNT/A3 TLDQNKQNIQRVVFKYSQMVNISDYINRWIEVITNNRRLTKSKYIINGRLIDQKPIISNLG
 BoNT/A4 TLDQTQEIQRVVFKYSQMINISDYINRWIEVITNNRRLTKSKYIINGRLIDQKPIISNLG
 BoNT/A5 TLDQNKQNIQRVVFKYSQMVNISDYINRWIEVITNNRRLNNSKIYINGRLIDQKPIISNLG
 BoNT/A6 TLDQNKQNIQRVVFKYSQMVNISDYINRWIEVITNNRRLTKSKYIINGRLIDQKPIISNLG
 BoNT/A7 TLDQNKQNIQRVVFKYSQMVNISDYINRWIEVITNNRRLTKSKYIINGRLIDQKPIISNLG
 BoNT/A8 TLDQNKQNIQRVVFKYSQMVNISDYINRWIEVITNNRRLTKSKYIINGRLIDQKPIISNLG
 BoNT/HA TLDTEGIKKTVVVQYTCNINISDYINRWIEVITNNRRLNNSKIYINGRLINEESISDLG

1050 1060 1070 1080 1090 1100

BoNT/A1 NIHASNNIMFKLDGCRDTHRYIWKIYFNLFDKELNEKEIKDLYDNOSNSGILKDFWGDYLD
 BoNT/A2 NIHASNKIMFKLDGCRDPRRYIMIKYFNLFDKELNEKEIKDLYDSOSNSGILKDFWGNLYL
 BoNT/A3 NIHASNKIMFKLDGCRDPRRYIMIKYFNLFDKELNEKEIKDLYDSOSNSGILKDFWGNLYL
 BoNT/A4 NIHASNKIMFKLDGCRDPRRYIVIKYFNLFDKELSEKEIKDLYDNOSNSGILKDFWGDYLD
 BoNT/A5 NIHASNNIMFKLDGCRDTHRYIWKIYFNLFDKELNEKEIKDLYDNOSNSGILKDFWGNLYL
 BoNT/A6 NIHASNKIMFKLDGCRDPRRYIMIKYFNLFDKELNEKEIKDLYDSOSNSGILKDFWGNLYL
 BoNT/A7 NIHASNKIMFKLDGCRDPRRYILIKYFNLFDKELNEKEIKDLYDNOSNSGILKDFWGDYLD
 BoNT/A8 NIHASNNIMFKLDGCRDPRRYIVIKYFNLFDKELNEKEIKDLYDNOSNSGILKDFWGDYLD
 BoNT/HA NIHASNNIMFKLDGCRDPRRYIWKIYFNLFDKELNKEIKDLYDNOSNSGILKDFWGDYLD

1110 1120 1130 1140 1150 1160

BoNT/A1 QYDKPYMNLNLYDPNKYVDVNNVGIKGYMYLKGPRGSMVTNIIYLNLSLYMGTKFFIHKY
 BoNT/A2 QYDKPYMNLNLYDPNKYVDVNNIIGIRGYMYLKGPRGSMVTNIIYLNLSLYMGTKFFIHKY
 BoNT/A3 QYDKPYMNLNLYDPNKYVDVNNIIGIRGYMYLKGPRGSMVTNIIYLNLSLYMGTKFFIHKY
 BoNT/A4 QYDKPYMNLNLYDPNKYVDVNNVGIKGYMYLKGPRDVMVTNIIYLNLSLYMGTKFFIHKY
 BoNT/A5 QYDKPYMNLNLYDPNKYVDVNNVGIKGYMYLKGPRGSMVTNIIYLNLSLYMGTKFFIHKY
 BoNT/A6 QYDKPYMNLNLYDPNKYVDVNNVGIKGYMYLKGPRSTLTTNIIYLNLSLYMGTKFFIHKY
 BoNT/A7 QYDKPYMNLNLYDPNKYVDVNNIIGIRGYMYLKGPRGSMVTNIIYLNLSLYMGTKFFIHKY
 BoNT/A8 QYDKPYMNLNLYDPNKYVDVNNIIGIRGYMYLKGPRGSMVTNIIYLNLSLYMGTKFFIHKY
 BoNT/HA QYDKPYMNLNLYDPNKYVDVNNVGIKGYMYLKGPRGSMVTNIIYLNLSLYMGTKFFIHKY

▲▲▲▲▲

1170 1180 1190 1200 1210 1220

BoNT/A1 ASGNKDNIVRNDRVYINVVVKNKEYRLATNASQAGVEKILSALEIPDVGNLSQVVMKSS
 BoNT/A2 ASGNKDNIVRNDRVYINVVVKNKEYRLATNASQAGVEKILSALEIPDVGNLSQVVMKSS
 BoNT/A3 ASGNKDNIVRNDRVYINVVVKNKEYRLATNASQAGVEKILSALEIPDVGNLSQVVMKSS
 BoNT/A4 ASGNKDNIVRNDRVYINVVVKNKEYRLATNASQAGVEKILSALEIPDVGNLSQVVMKSS
 BoNT/A5 ASGNKDNIVRNDRVYINVVVKNKEYRLATNASQAGVEKILSALEIPDVGNLSQVVMKSS
 BoNT/A6 ASGNKDNIVRNDRVYINVVVKNKEYRLATNASQAGVEKILSALEIPDVGNLSQVVMKSS
 BoNT/A7 ASGNKDNIVRNDRVYINVVVKNKEYRLATNASQAGVEKILSALEIPDVGNLSQVVMKSS
 BoNT/A8 ASGNKDNIVRNDRVYINVVVKNKEYRLATNASQAGVEKILSALEIPDVGNLSQVVMKSS
 BoNT/HA ASGNKDNIVRNDRVYINVVVKNKEYRLATNASQAGVEKILSALEIPDVGNLSQVVMKSS

1230 1240 1250 1260 1270 1280

BoNT/A1 KNDQGITNKKCKMNLQDNNNGNDIGFIFGHQFNNTAKLIVASNWYNROIGKASRRTLGCSEWFI
 BoNT/A2 KDDQGITRNKCKMNLQDNNNGNDIGFIFGHLYDNIAKLIVASNWYNROVGGKASRRTLGCSEWFI
 BoNT/A3 KDDQGITRNKCKMNLQDNNNGNDIGFVGFHLYDNIAKLIVASNWYNROVGGKASRRTLGCSEWFI
 BoNT/A4 KNDQGITNKKCKMNLQDNNNGNDIGFIFGHQFNNTAKLIVASNWYNROIGKASRRTLGCSEWFI
 BoNT/A5 KNDQGITRNKCKMNLQDNNNGNDIGFIFGHQFNNTIDKLIVASNWYNROIGKASRRTLGCSEWFI
 BoNT/A6 KNDQGITRNKCKMNLQDNNNGNDIGFIFGHKFNIDIKLIVASNWYNROIEISRRTLGCSEWFI
 BoNT/A7 KNDQGITRNKCKMNLQDNNNGNDIGFIFGHQFNNTAKLIVASNWYNROIGKASRRTLGCSEWFI
 BoNT/A8 KNDQGITRNKCKMNLQDNNNGNDIGLIGFHFQFNNTAKLIVASNWYNROVGGKASRRTLGCSEWFI
 BoNT/HA ENDQGITRNKCKMNLQDNNNGNDIGFIFGHQFNNTAKLIVASNWYNROIGKASRRTLGCSEWFI

1290

BoNT/A1 PVDDCWGERPFL
 BoNT/A2 PVDDCWGESL
 BoNT/A3 PVDDCWGESL
 BoNT/A4 PVDDCWGERPFL
 BoNT/A5 PVDDCWGESFL
 BoNT/A6 PVDDCWGESFL
 BoNT/A7 PVDCWGESL
 BoNT/A8 PVDDCWGESL
 BoNT/HA PVDDCWGESL

★ ★ ★ ▲

Supplementary Figure 9

Sequence alignment among eight BoNT/A subtypes and BoNT/HA.

The amino acid sequence of BoNT/A1-A8 and HA are taken from GenBank: AAQ06331.1 (A1), ACO83782.1 (A2), ABA29017.1 (A3), ACQ51417.1 (A4), ACG50065.1 (A5), ACW83608.1 (A6), AFV13854.1 (A7), AJA05787.1 (A8), and KGO15617.1 (HA). Sequence alignments were made using Clustal Omega ¹ and ESPript ². Identical residues are indicated with white letters on a red background, similar conserved residues are in red letters, varied residues are in black letters. Key H_CA residues that are recognized by antibody CR1 (PDB code: 2NYY) ⁵ are indicated by black stars. H_CA residues that directly interact with SV2C peptide or the N559-glycan are labeled by blue triangles or yellow ovals, respectively.

Supplementary Table 1

Water-mediated interactions in the SV2C glycan-HcA interface

Water #	Distance (Å)	Water #	SV2C N559-glycan	HcA (or SV2C)
W1	3.15	W2		
	3.04			F953 [N]
	3.04			N954 [N]
	2.79			S957 [OG]
	2.97			D1062 [OD2]
W2	2.90		NAG603 [O7]	
	2.67			D1062 [OD2]
	2.76			R1065 [NH2]
W3	2.62		NAG603 [O3]	
	3.15		BMA604 [O6]	
	2.77			H1064 [O]
W4	2.84		FUC601 [O2]	
	3.39		NAG602 [O6]	
	2.70		NAG603 [N2]	
	2.66			D1289 [O]
W5	2.61		FUC601 [O2]	
	3.40		FUC601 [O3]	
	2.69			D1289 [OD1]
W6	2.79	W7		
	2.66			Y1155 [OH]
	2.84			D1288 [O]
	3.02			G1292 [N]
W7	2.84		FUC601 [O4]	
	3.38		FUC601 [O5]	
	2.60			E1293 [O]
W8	3.32		NAG602 [O7]	
	2.80			D539 [OD2] – SV2C
W9	2.95	W10		
	2.96			F953 [O]
	2.67			T1145 [OG1]
	3.12			N559 [OD1] – SV2C
W10	2.36		NAG602 [N2]	

REFERENCES

1. Sievers, F. et al. Fast, scalable generation of high-quality protein multiple sequence alignments using Clustal Omega. *Mol Syst Biol* **7**, 539 (2011).
2. Gouet, P., Courcelle, E., Stuart, D.I. & Metz, F. ESPript: analysis of multiple sequence alignments in PostScript. *Bioinformatics* **15**, 305-8 (1999).
3. Laskowski, R.A. & Swindells, M.B. LigPlot+: multiple ligand-protein interaction diagrams for drug discovery. *J Chem Inf Model* **51**, 2778-86 (2011).
4. Lo, M.C. et al. Evaluation of fluorescence-based thermal shift assays for hit identification in drug discovery. *Anal Biochem* **332**, 153-9 (2004).
5. Garcia-Rodriguez, C. et al. Molecular evolution of antibody cross-reactivity for two subtypes of type A botulinum neurotoxin. *Nat Biotechnol* **25**, 107-16 (2007).